The Early Cretaceous San Juan Plutonic Suite, Ecuador: a magma chamber in an oceanic plateau?

Marc Mamberti, Henriette Lapierre, Delphine Bosch, Etienne Jaillard, Jean Hernandez, and Mireille Polvé

Abstract: Sections through an oceanic plateau are preserved in tectonic slices in the Western Cordillera of Ecuador (South America). The San Juan section is a sequence of mafic–ultramafic cumulates. To establish that these plutonic rocks formed in an oceanic plateau setting, we have developed criteria that discriminate intrusions of oceanic plateaus from those of other tectonic settings. The mineralogy and crystallization sequence of the cumulates are similar to those of intra-plate magmas. Clinopyroxene predominates throughout, and orthopyroxene is only a minor component. Rocks of intermediate composition are absent, and hornblende is restricted to the uppermost massive gabbros within the sequence. The ultramafic cumulates are very depleted in light rare-earth elements (LREE), whereas the gabbros have flat or slightly enriched LREE patterns. The composition of the basaltic liquid in equilibrium with the peridotite, calculated using olivine compositions and REE contents of clinopyroxene, contains between 16% and 8% MgO and has a flat REE pattern. This melt is geochemically similar to other accreted oceanic plateau basalts, isotropic gabbros, and differentiated sills in western Ecuador. The Ecuadorian intrusive and extrusive rocks have a narrow range of εNd_i (+8 to +5) and have a rather large range of Pb isotopic ratios. Pb isotope systematics of the San Juan plutonic rocks and mineral separates lie along a mixing line between the depleted mantle (DMM) and the enriched-plume end members. This suggests that the Ecuadorian plutonic rocks generated from the mixing of two mantle sources, a depleted mid-oceanic ridge basalt (MORB) source and an enriched one. The latter is characterized by high $(^{207}Pb/^{204}Pb)_i$ ratios and could reflect a contamination by recycled either lower continental crust or oceanic pelagic sediments and (or) altered oceanic crust (enriched mantle type I, EMI). These data suggest that the San Juan sequence represents the plutonic components of an Early Cretaceous oceanic plateau, which accreted in the Late Cretaceous to the Ecuadorian margin.

Résumé : Des sections transversales d'un plateau océanique sont préservées dans des tranches tectoniques de la cordillère ouest de l'Équateur (Amérique du Sud). La section San Juan est une séquence de cumulats mafiques-ultramafiques. Afin de déterminer si ces roches plutoniques forment un environnement de plateau océanique, nous avons développé des critères qui différencient les intrusions de plateaux océaniques des autres environnements tectoniques. La minéralogie et la séquence de cristallisation des cumulats sont semblables à celles des magmas intraplaques. Le clinopyroxène prédomine partout et l'orthopyroxène n'est qu'une composante mineure. Les roches de composition intermédiaire sont absentes et la hornblende est limitée aux gabbros massifs au sommet de la séquence. Les cumulats ultramafiques sont très appauvris en éléments de terres rares légers (LREE), alors que les gabbros ont des spectres LREE plats ou légèrement enrichis. La composition du liquide basaltique en équilibre avec la péridotite, calculée en utilisant les compositions d'olivine et le contenu en éléments de terres rares du clinopyroxène, contient entre 16 et 8 % MgO et a un spectre d'éléments de terres rares plat. Ces produits fondus sont géochimiquement semblables à d'autres accrétions de basaltes de plateau océanique, de gabbros isotropes et de filons-couches différenciés dans l'ouest de l'Équateur. La plage de εNd_i (+8 à +5) des roches équatoriennes intrusives et extrusives est étroite et la plage des rapports des isotopes du Pb est plutôt large. La systématique des isotopes du Pb des roches plutoniques et des minéraux isolés de San Juan est répartie le long d'une ligne de mélange entre le manteau appauvri (DMM) et les panaches enrichis des membres des extrémités. Cela nous porte à croire que les roches plutoniques équatoriennes découlent du mélange de deux sources mantelliques, un basalte médio-océanique (MORB) appauvri et un autre enrichi. Ce dernier est caractérisé

Received 12 January 2004. Accepted 15 July 2004. Published on the NRC Research Press Web site at http://cjes.nrc.ca on 27 October 2004.

Paper handled by Associate Editor J.D. Greenough.

M. Mamberti.[1] Institut für Mineralogie, Universität Hannover, Calinstrasse 3, 30167 Hannover, Deutschland.
H. Lapierre. Laboratoire Géodynamique des Chaînes Alpines, UMR-CNRS 5025, Université Joseph Fourier, Maison des Géosciences, B.P. 53, 38041 Grenoble CEDEX, France.
D. Bosch. Laboratoire de Tectonophysique, UMR-CNRS 5568, CC 066, Univesité Montpellier II, Place Eugène Bataillon, 34095 Montpellier CEDEX 05, France.
E. Jaillard. IRD, CSS1, 209–213 Rue la Fayette, 75480 Paris CEDEX 10, France.
J. Hernandez. Institut de Minéralogie, Université de Lausanne, BFSH2 UNIL-Dorigny, 1015 Lausanne, Switzerland.
M. Polvé. UMR-CNRS 5563, Université Paul Sabatier, 38 Rue des 36 Ponts, 31400 Toulouse, France.

[1]Corresponding author (e-mail: m.mamberti@mineralogie.uni-hannover.de).

 doi: 10.1139/E04-060

par des rapports ($^{207}Pb/^{204}Pb$) élevés et pourrait refléter une contamination par des roches recyclées provenant soit d'une croûte continentale inférieure ou de sédiments pélagiques océaniques et/ou d'une croûte océanique altérée (manteau enrichi de type 1). Des données suggèrent que la séquence de San Juan représente les composantes plutoniques d'un plateau océanique du Crétacé inférieur qui s'est accrété à la bordure équatorienne au Crétacé supérieur.

[Traduit par la Rédaction]

Introduction

Despite the enormous size of oceanic plateaus, very little is known about their overall structure and composition, especially about their deep crustal levels. Most major plateaus (Ontong Java, Nauru, Manihiki) are located in deep waters within the Pacific Ocean and their deeper parts are inaccessible. Deep-sea drilling has penetrated only their uppermost volcanic levels, which represent a minute fraction (<0.5%) of their total thickness (Saunders et al. 1996; Storey et al. 1991; Mahoney et al. 1993; Coffin and Eldholm 1993).

The best way to study the internal structure and composition of an oceanic plateau is to analyse the fragments of plateaus exposed through accretion onto plate margins. The best known examples are the 2–3 km-thick slices of volcanic rocks, obducted on the Solomon Islands, which are thought to have formed part of the Ontong Java plateau (Neal et al. 1997; Parkinson et al. 1996), and the fragments of the Caribbean oceanic plateau accreted along the Pacific coast of Central and South America and the Greater Antilles (Kerr et al. 1996*a*, 1996*b*, 1997*a*, 1997*b*, 1998; Sinton and Duncan 1997, 1998; Reynaud et al. 1999; Hauff et al. 2000*a*; Lapierre et al. 1997, 2000). The accreted fragments of oceanic plateau affinity most commonly consist of basalts and dolerites intruded by shallow level gabbros and probably represent the uppermost levels of the oceanic plateau. Among the few examples that are thought to come from the interior of oceanic plateaus are the ultramafic and mafic cumulates associated with komatiites and picrites of the Colombian oceanic plateau (Kerr et al. 1997*b*; Spadea et al. 1987; Révillon et al. 1999, 2000), and gabbros and peridotites of the Solomon Islands (Parkinson et al. 1996).

On the basis of different crustal sections, Kerr et al. (1997*b*, 1998) developed a model of the internal structure of the 90-Ma Caribbean plateau. In their model, large layered intrusive bodies are located just above or below the Moho. Those within the crust are plagioclase-rich cumulates, while the deeper levels are composed of peridotites, pyroxenites and olivine gabbros. To test this, we require more detailed information on the petrological and geochemical characteristics of intrusions that may represent relict magma chambers. In some of the examples just listed, there is little doubt that the intrusions are comagmatic with oceanic plateau basalts. This is the case for the intrusions of Gorgona Island, which have chemical compositions that link them definitively to the ultramafic lavas.

In this paper, we describe the petrological and geochemical characteristics of two suites of rocks from the Western Cordillera of Ecuador. The first suite is composed of pillow basalts, dolerites, and shallow-level gabbroic intrusions, while the second suite consists of cumulate ultramafic to mafic intrusive rocks. Because the geodynamic setting of the cumulate rocks is difficult to establish solely on the basis of their geochemistry, we have developed a set of criteria that helps to discriminate cumulate rocks belonging to an oceanic plateau from those developed in an intra-oceanic island-arc setting. Before using these criteria, we will test them against the features of plutonic complexes for which the tectonic environment is well constrained. We then use them to evaluate the geodynamic setting of the Ecuadorian ultramafic–mafic rocks and show that they did indeed form part of an oceanic plateau. Finally, we will propose a petrogenetic model for the intrusive suites and use this model to develop a description of the internal structure and evolution of an oceanic plateau.

Geological setting

Ecuador comprises three main morphological domains (Fig. 1). The first, the "Oriente" Basin, represents the present-day foreland basin of the Andean orogen. The second, the Ecuadorian Andes, comprises two cordillera, crosscut and overlain by the products of Tertiary–Recent magmatic arcs (Aspden and Litherland 1992; Lavenu et al. 1992). The Eastern Cordillera consists of deformed Paleozoic to Mesozoic metamorphic rocks (Litherland et al. 1994), while the Western Cordillera is composed of oceanic terranes that accreted to the Andean margin in the late Santonian to Eocene (Cosma et al. 1998; Hughes and Pilatasig 2002; Kerr et al. 2002*a*). The third domain, the Coastal Zone, consists of basalts and dolerites of oceanic plateau affinity, overlain by Late Cretaceous island-arc rocks (Goossens and Rose 1973; Lebrat et al. 1987; Jaillard et al. 1997; Reynaud et al. 1999).

Two lithological associations have been recognized in the accreted oceanic terranes. Type 1 is composed of massive and pillowed mafic lava flows, tuffs, and greywackes intruded by shallow-level gabbros and dolerites. This type is widely exposed on Piñon Formation in the coast (Reynaud et al. 1999; Fig. 1) and in the Western Cordillera, where it is called the Pallatanga Unit (Dunkley and Gaibor 1998; Kerr et al. 2002*a*; Hughes and Pilatasig 2002).

The second lithological association (Type 2) consists of cumulate peridotites and gabbros intruded by mafic and felsic dykes (Fig. 2). This type is well exposed along the 2000 m-thick San Juan section, one of several tectonic slices pinched in a Late Cretaceous suture near the crest of the Western Cordillera. The section has been interpreted by Juteau et al. (1977) as an oceanic crustal remnant, and by Desmet (1994) and Lapierre et al. (2000) as part of an oceanic plateau. The San Juan section appears to represent a complete cumulate suite with massive dunites at the base, grading upwards through layered wehrlites and gabbros into isotropic amphibole gabbros (Fig. 2).

These two lithologic sequences are Late Cretaceous in age. In the coastal zone, the Piñon Formation is regarded as

Fig. 1. Schematic geological map of Ecuador showing the main geological and tectonic units and the location of the San Juan section. This section of the Western Cordillera of Ecuador represent Lower Cretaceous oceanic fragments accreted to the Ecuadorian margin in the Late Cretaceous.

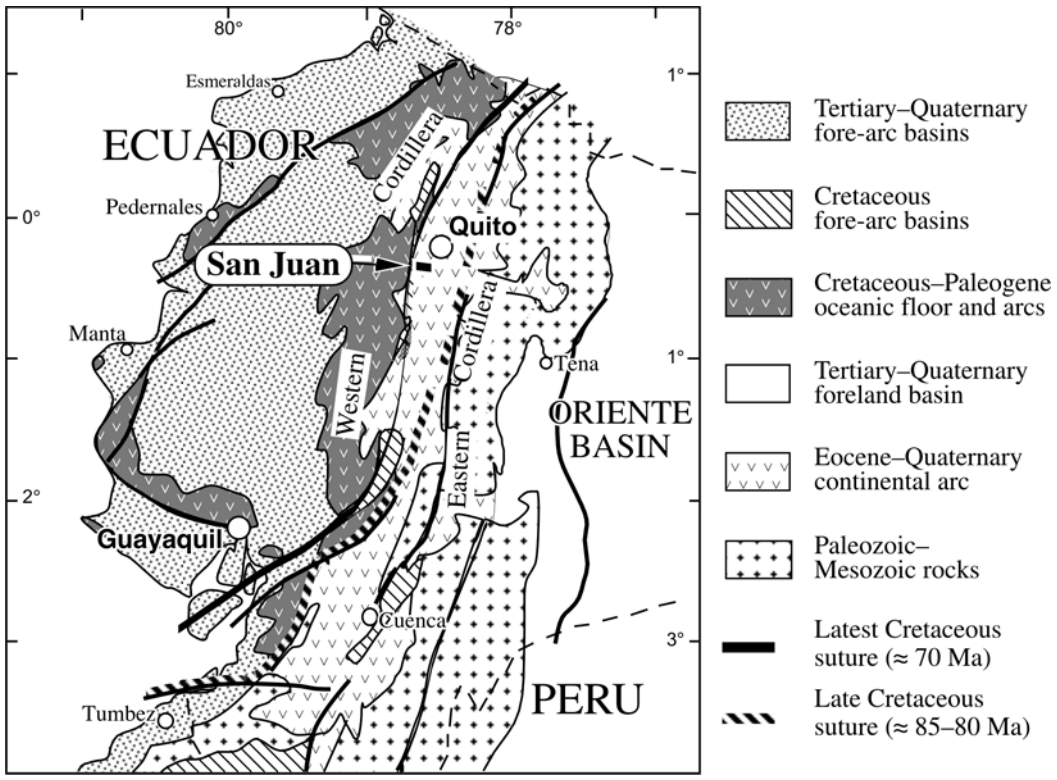

pre-Late Cretaceous, since it forms the basement to undated volcanic arc rocks, which in turn are stratigraphically overlain by pelagic sediments containing Late Cretaceous faunas (late Campanian and Maastrichtian microfauna; Jaillard et al. 1995). An amphibole-bearing gabbro from the San Juan section (Type 2) has been dated by Lapierre et al. (2000) who obtained an internal Sm–Nd isochron age of 123 ± 13 Ma, whereas amphiboles of the same gabbro yielded a poor Ar/Ar plateau age of 99.2 ± 1.3 Ma and an integrated age of 105 Ma (Fig. 3). This Late Cretaceous age is unknown in the Caribbean–Colombian oceanic plateau where the main volcanic pulse occurred during the Late Cretaceous (90–86 Ma).

Several mafic rocks were sampled from different sections considered to belong to the Late Cretaceous oceanic plateau exposed in the Western Cordillera (Mamberti et al. 2003). In spite of the thorough survey and mapping of Hughes et al. (1999), most of the exposed sections consist of basaltic lava flows intruded by sills; cumulus ultramafic and mafic rocks have only been described in the San Juan section.

Petrology and mineral chemistry of the San Juan section (Type 2)

Four units are recognized in the San Juan section (Type 2), each bounded by northeast-trending normal or reverse faults (Fig. 2). From to east to west the units are

(1) fine- to coarse-grained, isotropic, amphibole-bearing gabbros (97SJ13) intruded by pegmatitic gabbros and swarms of basaltic, doleritic, and calc-alkaline dacitic dykes. Locally, plagioclase in the gabbros exhibits an igneous lamination. An upper faulted contact separates the gabbros from overlying Pliocene to Quaternary felsic tuffs.

(2) layered cumulate olivine gabbros (97SJ1, 97SJ3) and two-pyroxene gabbros (97SJ4, 97SJ9) intruded by rare and thin basaltic and doleritic dykes. The latter display arc-tholeite affinities (Mamberti 2001).

(3) layered cumulate fine-grained peridotites (97SJ6, 97SJ8, 97SJ10, 98SJ4) with locally abundant clinopyroxene or interstitial plagioclase. Clinopyroxene-rich rocks are coarse-grained.

(4) massive partially serpentinized peridotites (98SJ2) crosscut by gabbroic and ultramafic (98SJ3) dykes, locally affected by shear zones.

Four rock types have been distinguished on the basis of their textures, mineralogy, and petrology. The petrographic characteristics of these plutonic rocks are summarized in Table 1. In order of decreasing abundance they are (1) cumulate peridotites, (2) layered olivine–clinopyroxene gabbros, (3) isotropic amphibole gabbros, (4) dykes. The crystallization sequence of the San Juan cumulate rocks is olivine followed by clinopyroxene and plagioclase.

All the rocks are hydrothermally altered. Although olivine cores are preserved in some peridotites and gabbros, most grains are intensely fractured and almost completely serpentinized. Orthopyroxene is commonly replaced by chlorite and (or) smectite. In contrast, clinopyroxene is preserved in most samples, except in some peridotites and gabbros in which it is replaced by actinolite. Plagioclase is fresh in the gabbros but is variably altered in the peridotites and

Fig. 2. Schematic cross section of the San Juan plutonic sequence showing the different components of the deep levels of the Early Cretaceous Ecuadorian oceanic plateau.

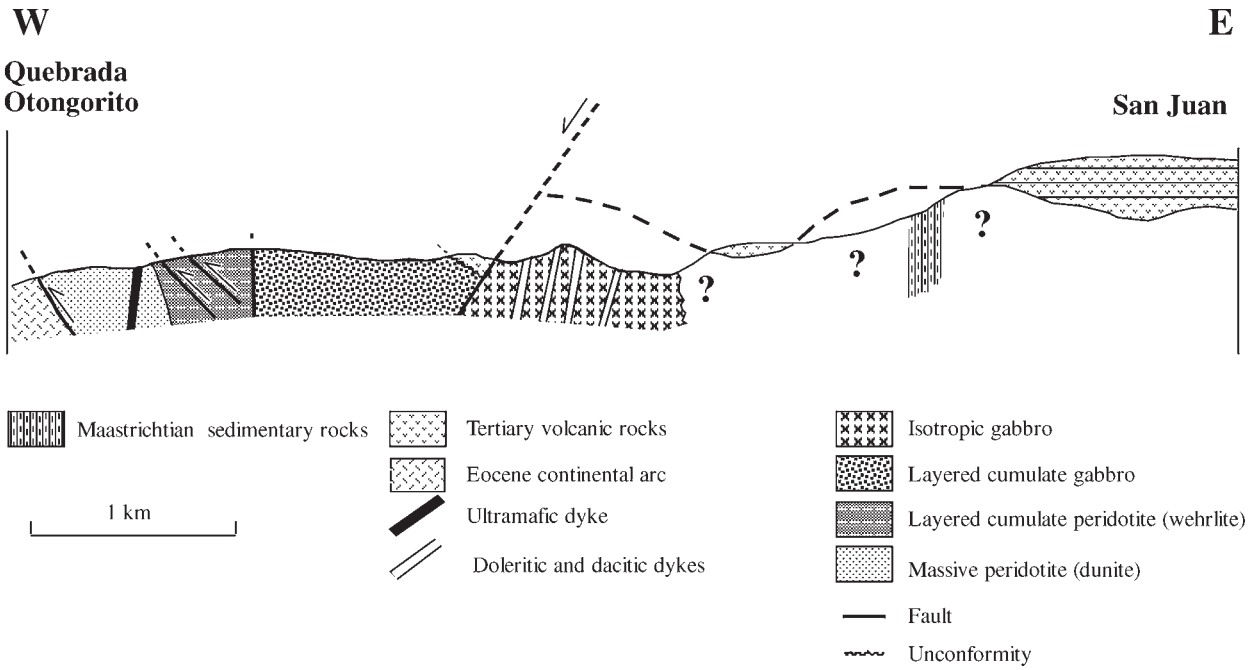

dolerites. In peridotites, it is replaced by a microcrystalline assemblage of hydrogarnet and epidote. Fe–Ti oxides are preserved in the gabbros.

Peridotite

The peridotites are either massive or layered, and include both dunites and wehrlites. The dunites (98SJ2) are unlayered and consist of very fine grained serpentinized olivine, euhedral chromite grains ($0.50 < Cr\# = Cr/(Cr + Al) < 0.57$), and interstitial diopside (En_{48} Fs_5 Wo_{47}) (Morimoto 1988). When preserved, cumulus olivine is forsteritic ($Fo_{89–91}$). Wehrlites (SJ33, 98SJ4, 97SJ8, 97SJ10) are layered with mineral banding formed by olivine and clinopyroxene with local interstitial, late-crystallizing plagioclase. They are mesocumulates with cumulus olivine and clinopyroxene and plagioclase as the intercumulus phase. Olivine composition is very constant (Fo_{84}) with no chemical variations between core and rim. The pyroxene is diopside ($Wo_{45–48}$ $En_{44–47}$ $Fs_{5–7}$) with a very uniform composition. When preserved, plagioclase is always bytownite ($An_{87–88}$), regardless the type of associated mineral (olivine or clinopyroxene). Variations in the wehrlite are expressed by the abundance of the plagioclase and the presence of clinopyroxene exsolution lamelles within the diopside. The wehrlites contain isolated layers predominantly of plagioclase with some cumulus olivine (97SJ6).

Layered gabbro

The layered gabbros contain two pyroxenes with or without olivine. The olivine gabbros (97SJ2, 97SJ3) are adcumulates with olivine, plagioclase, and clinopyroxene as cumulus phases and orthopyroxene and plagioclase as the intercumulus phase. Olivine included in the pyroxenes is forsteritic but more Mg-rich (Fo_{75}) than that in the wehrlites. Among the cumulus crystals, plagioclase predominates and displays an adcumulate texture.

The olivine-free gabbros (97SJ4, 97SJ9 and SJ40) show three distinctly different facies. 97SJ9 differs from the olivine gabbros solely by the absence of olivine. 97SJ4 differs significantly from the other gabbros by the crystal sequence and the exceptional preservation of orthopyroxene (clinoenstatite; Wo_{28} En_{71} Fs_1). In this rock, both pyroxenes crystallized before the plagioclase. Two generations of Fe–Ti oxides are present. The early crystallizing oxides consist of small euhedral crystals included in the pyroxenes, while the late ones occur as large interstitial grains. SJ40 differs from 97SJ4 and 97SJ9 by the presence of clinopyroxene partly replaced by hornblende and scarce (5%) orthopyroxene pseudomorphs.

Regardless of the gabbro lithologies, both clinopyroxene ($Wo_{45–47}$ $En_{44–45}$ $Fs_{8–9}$) and plagioclase ($An_{84–88}$) have uniform and constant compositions that do not differ from those in the wehrlites.

Amphibole-bearing gabbro (97SJ13)

These unlayered rocks are coarser grained than the cumulate gabbros and contain more sodic plagioclase ($An_{52–44}$). This mineral forms large (<1 cm) crystals rimmed by brown pleochroic Mg-rich amphibole. Inclusions of clinopyroxene and smaller plagioclase crystals are common. The amphibole is Mg-rich hornblende (Leake et al. 1997).

Analytical methods

All the igneous rocks have been hydrothermally altered and metamorphosed to greenschist facies; the plutonic rocks are, however, less altered than the basalts. For this reason, only samples with well-preserved igneous mineralogy (i.e., clinopyroxene, amphibole, and plagioclase) and devoid of significant petrographic alteration were selected for chemical analysis. Minerals were separated then purified by hand

Fig. 3. $^{40}Ar/^{39}Ar$ step-heating spectrum for 97SJ13 amphibole. Integrated age is the age taking into account all the Ar released. Analysis performed at the University of Lausanne, Switzerland.

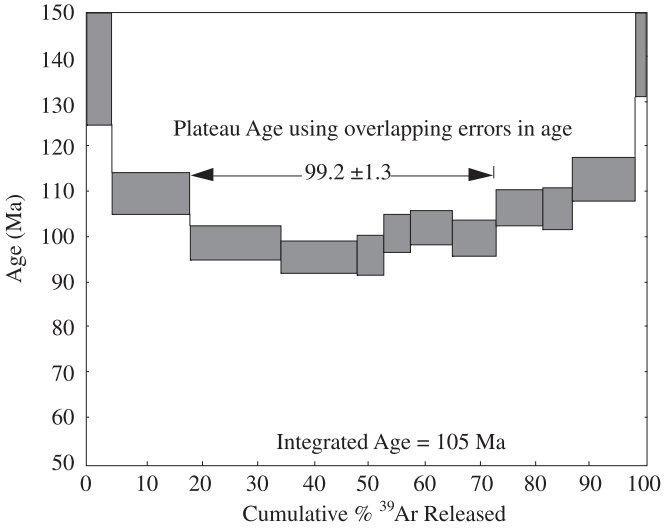

picking. Most mineral separates were 99% pure; actinolite rims around some clinopyroxene crystals, however, could not be completely removed.

Major-element analyses were performed by X-ray fluorescence at the Department of Geology of the Australian National University (Canberra) and at the Institut de Minéralogie et Pétrographie de l'Université de Lausanne (Switzerland). After acid dissolution, trace elements were analysed by inductively coupled plasma – mass spectrometry (ICP–MS) at the University of Grenoble (France) using a Tm spike following procedures described by Barrat et al. (1996). Standards used for the analyses were JB2, WSE, BIR-1, JR1, and UBN. The accuracy on trace-element concentrations is better than 5% (probably better than 3% for all the REEs based on various standards and sample duplicate). Major- and trace-element analyses of the minerals and host rocks are presented in Tables 2 and 3.

For Sr and Nd isotopic analyses, mineral separates and host rock powders were leached in a mixture of 2 N HCl and 0.1 N HF. Sr (static acquisition) and Nd (dynamic acquisition) isotopic ratios were measured at the Laboratoire de Géochimie isotopique de l'Université Paul Sabatier de Toulouse, France (Table 4) on a Finnigan MAT261 multicollector mass spectrometer using the analytical procedures described by Lapierre et al. (1997). Results on standards yielded $^{143}Nd/^{144}Nd$ = 0.511850 ± 0.000017 on 12 standards analysed. Results on NBS 987 Sr standard yielded $^{87}Sr/^{86}Sr$ = 0.710250 ± 0.000030 on 11 standard determinations. $^{87}Sr/^{86}Sr$ and $^{143}Nd/^{144}Nd$ were normalized for mass fractionation relative to $^{86}Sr/^{88}Sr$ = 0.1194 and $^{146}Nd/^{144}Nd$ = 0.7219, respectively.

For lead separation, powdered samples were weighted to obtain ~200 ng of lead. A leaching step with 6N HCl during 30 min at 65 °C was done before acid digestion. Samples were then dissolved during 48 h on a hotplate with a mixing of tridistilled HF:HNO_3 concentrated acids. After evaporation to dryness, 1 mL of HNO_3 was added to the residue and kept at about 90 °C for 12–24 h. After complete evaporation, 0.5 mL of 8N HBr was added to the sample, which was kept at 70 °C for 2–3 h before complete evaporation. The chemical separation of lead was carried out using 50 mL of anion exchange resin (AG1X8, 200–400 mesh) and samples were loaded and washed in 0.5N HBr. Lead was then eluted in 6N HCl. Pb blanks were < 40 pg and are negligible for the present analyses. Lead isotope analyses were made on a VG Plasma 54 multicollector inductively coupled plasma – mass spectrometer (MC–ICP–MS) at Ecole Normale Supérieure de Lyon, France. This MC–ICP–MS allows routinely high precision isotope ratio determinations. Lead isotope compositions were measured using the Tl normalization method described by White et al. (2000). For Pb isotope analysis, samples were bracketed between NIST 981 standards splits and calculated with respect to the value reported for this standard by Todt et al. (1996). This technique yields internal precision of ca. 50 ppm (2σ) and an external reproducibility of ca. 150 ppm (σ) for $^{206}Pb/^{204}Pb$ ratios determined on 20 NIST (National Institute of Standards) standards.

The complete isotopic data set has been corrected for in situ decay assuming an age of 123 Ma, based on the age of the (97SJ13) gabbro (Lapierre et al. 2000). εNd_i was calculated with $(^{143}Nd/^{144}Nd)_{CHUR}$ = 0.512638 and $(^{147}Sm/^{144}Nd)_{CHUR}$ = 0.1967 (Jacobsen and Wasserburg 1980; CHUR, chondritic uniform reservoir). εSr_i was calculated with $(^{87}Sr/^{86}Sr)_{CHUR}$ = 0.70450 and $(^{87}Rb/^{86}Sr)_{CHUR}$ = 0.084 (DePaolo 1988).

The $^{40}Ar/^{39}Ar$ analyses were carried out at the Université de Lausanne. Samples together with the standards were irradiated for 20 minutes in the Cadmium-Line in-Core Irradiation Tube in the central thimble position of the United States Geological Survey Triga reactor in Denver, Colorado (Dalrymple et al. 1981). Analytical method in Feeley et al. (2002).

Geochemistry

Major-element chemistry

Cumulate ultramafic rocks have higher MgO and Fe_2O_3 contents than the gabbros. In contrast, the cumulate ultramafic rocks, compared with the gabbros, are depleted in Al_2O_3 and SiO_2. Al_2O_3 contents of the wehrlites depend on the abundance of plagioclase and clinopyroxene. Ultramafic and mafic rocks have very low TiO_2 abundances with the exception of the isotropic gabbro (97SJ13). Major- and trace-element analyses of the cumulate rocks are reported in Table 3 and plotted in Figs. 4–7.

Mobility of major and trace elements

Before interpreting the chemistry of the San Juan igneous rocks in terms of magmatic processes, we have to assess the possible chemical effects of element mobility during hydrothermal alteration and metamorphism. The gabbros have low to moderate values of loss on ignition (LOI = 0.4%–5.4%), with the exception of the dunites and two wehrlites, in which most of the olivine is serpentinized (LOI = 8.4%–13.1%; Table 3).

Light rare-earth elements (LREE), such as Ce, are regarded as being relatively immobile during alteration of rocks of mafic to ultramafic compositions in the absence of Ca-rich fluids (Humphris 1984). In Fig. 4, Ce is plotted against Ba, Sr, and Rb, elements that are considered to be very mobile during alteration and low-grade metamorphism. Ba shows positive correlation, suggesting that Ba is rela-

Table 1. Petrographic description of the San Juan cumulate rocks.

A	Sample:	97SJ1	97SJ3	97SJ4	97SJ9	97SJ13
	Name:	Olivine gabbro	Olivine gabbro	Two-pyroxene gabbro	Two-pyroxene gabbro	Gabbro
	Texture:	Meso- to heteradcumulate	Meso- to heteradcumulate	Mesocumulate	Meso- to heteradcumulate	Granular
	Mineralogy:[a]	Plag cumulus (70%), ol cumulus (2%), cpx (20%) Intercumulus opx pseudomorphs (10%)	Plag cumulus (70%), ol cumulus (2%), cpx (20%), intercumulus opx pseudomorphs (10%)	Plags in cumulus (65%), Preserved cpx and opx (30%) in cumulus, late and early crystallizing Ti- and V-rich magnetite (5%)	Plag cumulus (60%), cpx cumulus (30%), intercumulus opx pseudomorphs (10%)	Plag (50%), amph with pyroxene core (50%)
B	Sample:	98SJ2	97SJ6	97SJ8	97SJ10	98SJ4
	Name:	Dunite	Plagioclase-rich wehrlite	Wehrlite	Wehrlite	Wehrlite
	Texture:	Heteradcumulate	Layered heteradcumulate	Layered heteradcumulate	Layered heteradcumulate	Layered heteradcumulate
	Mineralogy:	Ol (90%), cpx (5%), oxide (5%)	Mineral banding, ol (50%), cpx (40%), plags intercumulus (10%)	Ol (60%), cpx (30%), plags intercumulus (5%), oxide (< 1%)	Ol (70%), cpx (20%), plags intercumulus (5%), oxide (< 1%)	Ol (65%), cpx (30%), plags intercumulus (5%), oxide
C	Sample:	97SJ11	97SJ12			
	Name:	Dolerite	Rhyolite			
	Texture:	Ophitic	Intersertal-ophitic			
	Mineralogy:	Plags, cpx replaced by chlorite, interstitial quartz, Ti magnetite	Plag phenocrysts, quartz phenocrysts, epidote, Ti magnetite			

[a]amph, amphibole; cpx, clinopyroxene; opx, orthopyroxene; plag(s), plagioclase(s); ol, olivine.

Table 2. Major- (wt.%) and trace-element (ppm) analyses for the San Juan mineral separates.

Sample:	97SJ10	97SJ3	97SJ13	97SJ13
Name:[a]	Cpx	Cpx	Plag	Amph
Host rock:	Wehrlite	Gabbro	Gabbro	Gabbro
SiO_2	52.56	51.74	54.55	46.81
TiO_2	0.15	0.21	—	1.75
Al_2O_3	2.72	2.79	28.3	7.31
Fe_2O_3	—	—	—	9.92
FeO	4.03	5.67	0.4	6.36
MnO	0.02	0.04	—	0.3
MgO	16.99	15.58	—	13.72
CaO	22.33	22.84	10.7	11.12
Na_2O	0.31	0.34	5.44	1.3
K_2O	—	—	0.14	0.08
Total	99.1	99.2	99.53	100.59
Ba	0.91	5.73	86	29.54
Rb	0.11	0.1	1.43	0.49
Sr	4.21	9.67	223	17.6
Ta	bd	0.01	0.03	0.07
Th	0.21	0.03	0.05	0.08
Zr	2.22	4.71	1.23	37
Nb	0.04	0.1	0.05	1.47
Y	3.91	8.76	0.88	71
Hf	0.1	0.2	0.04	1.85
Co	87	51.64	5.87	70
U	0.01	0.02	0.02	0.03
La	0.18	0.26	1.44	2.44
Ce	0.5	1.16	2.41	11.48
Pr	0.11	0.25	0.28	2.7
Nd	0.6	1.43	0.92	16.22
Sm	0.29	0.58	0.17	6.35
Eu	0.15	0.22	0.43	1.38
Gd	0.41	0.87	0.23	7.97
Tb	0.09	0.18	0.03	1.63
Dy	0.66	1.31	0.14	11.24
Ho	0.15	0.31	0.03	2.59
Er	0.45	0.93	0.08	7.33
Tm	—	—	—	—
Yb	0.44	0.95	0.08	7.14
Lu	0.07	0.14	0.01	1.08

[a]Amph, amphibole; Cpx, clinopyroxene, Plag, plagioclase.

tively immobile. Sr correlates with Ce in the peridotites but remains constant as Ce increases in the gabbros. These trends reflect the crystallization of clinopyroxene followed by the accumulation of plagioclase. Rb does not correlate with Ce, suggesting that this element was mobile during the alteration that affected the San Juan cumulate rocks.

Magmatic processes

Plots of Al_2O_3, CaO, SiO_2, and FeO versus MgO (Fig. 5) show that (1) the San Juan ultramafic rocks were derived from the accumulation of olivine, clinopyroxene, and plagioclase, and (2) the gabbros are formed by the accumulation of plagioclase followed by the crystallization of clinopyroxene. The gabbros 97SJ4 and 97SJ13 do not follow the general trend. The two-pyroxene gabbro 97SJ4 is distinguished from the other gabbros by evidence of cumulus orthopyroxene, as indicated by higher FeO and MgO, and lower CaO, contents. The hornblende gabbro 97SJ13 has much higher TiO_2, SiO_2, and lower MgO and represents a differentiated basalitc melt (Fig. 6).

Trace-element abundances in the mineral separates and host peridotites and gabbros are presented in Fig. 7. All the peridotites are markedly depleted in light relative to heavy REE (HREE), with the exception of 97SJ10, which shows a slight enrichment in La and Ce relative to Nd. Compared to its wehrlitic host rock, the cumulus clinopyroxene 97SJ10 has higher REE contents (chondritic values) and is more depleted in LREE. 97SJ10 and 98SJ4 are distinguished from the other peridotites by their marked positive Eu anomalies.

Trace-element contents in peridotites are very low. Most of the wehrlites and the clinopyroxene from sample 97SJ10 exhibit marked depletion in Nb, Ta, Zr, and Hf relative to the REE. The exception is the 97SJ10 whole-rock sample, which has near-chondritic contents of the Nb–Ta and Zr–Hf.

Three gabbros (97SJ1, 97SJ3, and 97SJ9) have flat REE patterns and marked Eu positive anomalies. Compared to its host rock, the cumulus clinopyroxene from 97SJ3 is depleted in LREE. 97SJ4 and 97SJ13 are LREE-enriched and LREE-depleted, respectively. The REE pattern of the 97SJ13 hornblende differs from its host rock by higher REE contents, a marked LREE-depletion and a negative Eu anomaly (Fig. 7). In contrast, the 97SJ13 plagioclase is strongly enriched in LREE and has a large positive Eu anomaly. SJ40 differs from all the gabbros by a marked depletion in LREE (less the chondritic values), while its Eu positive anomaly is similar to that of 97SJ1, 97SJ3, and 97SJ9.

The gabbros also show relative depletion of Ta, Nb, Zr, Hf, and Ti and enrichment of Ba and Sr. The exception is sample 97SJ4, which does not have these anomalies. The hornblende gabbro 97SJ13 and its amphibole and plagioclase separates have the highest trace-element abundances (Fig. 7). Plagioclase from 97SJ13 exhibits negative Nb, Zr, and Hf anomalies and is enriched in Sr and Eu. Amphibole from the same sample is enriched in Nb and Ta and depleted in Sr. The whole-rock sample 97SJ4 shows a positive Ti anomaly and a less marked depletion in Zr and Hf. The high Ti and Fe contents (Table 3) of this rock are explained by the presence of abundant Ti-rich magnetites.

The ultramafic dyke (98SJ3), which cuts across the massive peridotites, has a major-element composition similar to the 98SJ2 dunite (Table 3; Fig. 7), but has a flat LREE pattern and is enriched in HREE relative to the LREE, in contrast to the depleted LREE patterns of the peridotites.

Nd, Sr, Pb isotope chemistry

The wehrlites have a large range of εNd_i values, from +3.2 to +8.1 (Table 4; Fig. 8). These values overlap those of the gabbros (+5.2 to +7.5). Plagioclase and amphibole separated from sample 97SJ13 have uniform εNd_i ratios (+7.7 and +7.3), which are slightly higher than that of their host rock (+6.9). Clinopyroxene from 97SJ10 has an εNd_i ratio of +3.0, significantly lower than its host rock (+6.5). This is probably linked to the presence of actinolite that was not

Table 3. Major (wt.%) and trace element (ppm) analyses for the San Juan rock samples.

Sample:	98SJ2	97SJ6	97SJ8	97SJ8	97SJ10	97SJ10	98SJ4	97SJ33	97SJ1	97SJ3	97SJ4	97SJ9	97SJ13	97SJ40	98SJ3
Name:	Dunite	Wehrlite	Wehrlite*	Duplicate	Wehrlite*	Duplicate	Wehrlite	Wehrlite**	Gabbro	Gabbro	Gabbro	Gabbro	Gabbro	Gabbro**	Ultramafic dyke
SiO_2	40.7	47.01	46.9	—	44.53	—	42.82	42.96	48.15	48.13	48.05	48.21	52.38	49.61	40.57
TiO_2	0.03	0.1	0.09	—	0.06	—	0.04	0.04	0.06	0.06	0.20	0.06	0.42	0.07	0.02
Al_2O_3	1.60	8.39	7.85	—	6.81	—	7.34	6.55	23.33	22.8	6.47	22.32	20.4	16.33	1.02
Fe_2O_3	10.65	7.4	7.75	—	10.17	—	9.58	12.68	3.79	3.8	14.61	3.64	6.10	6.32	11.37
MnO	0.17	0.14	0.14	—	0.17	—	0.15	0.16	0.08	0.08	0.23	0.08	0.11	0.08	0.17
MgO	45.79	24.22	25.08	—	30.59	—	32.76	32.55	8.14	7.97	23.64	8.04	5.77	12.48	46.8
CaO	1.07	12.39	11.91	—	7.51	—	7.30	6.12	16.30	16.06	6.21	16.55	12.08	14.88	0.04
Na_2O	0.00	0.32	0.26	—	0.14	—	0.00	0.08	1.06	1.07	0.42	1.07	2.60	0.74	0.00
K_2O	0.01	0.01	0.01	—	0.02	—	0.00	0.01	0.01	0.02	0.17	0.01	0.12	0.04	0.00
P_2O_5	0.01	0.00	0.00	—	0.00	—	0.01	—	0.02	0.01	0.00	0.02	0.02	—	0.01
Total	100	100	100	—	100	—	100	100	100	100	100	100	100	100	100
LOI	13.11	3.54	5.43	—	6.88	—	8.39	—	0.92	1.04	0.38	0.86	0.74	—	3.34
Ba	2.85	4.18	—	3.83	—	5.38	3.55	4.76	6.57	15.2	33.9	5.57	113.1	9.25	5.56
Rb	0.14	0.10	0.30	0.29	0.4	0.32	0.13	0.22	0.13	0.25	4.07	0.31	1.50	0.34	0.10
Sr	3.89	29.2	32.3	33.6	21	24.9	13.0	23	108.9	110.7	42.9	113.7	154.9	87	2.68
Ta	nd	nd	nd	nd	0.01	nd	nd	0.05	nd	nd	0.02	nd	0.02	0.09	nd
Th	nd	nd	nd	nd	0.01	nd	nd	0.01	nd	0.01	0.4	nd	0.11	0.01	nd
Zr	nd	1.2	nd	1.27	2.10	2.03	nd	0.76	0.65	0.79	6.99	1.25	19.6	0.91	0.40
Nb	nd	nd	nd	0.03	0.30	0.22	nd	0.19	0.02	0.05	0.45	0.04	0.55	0.17	nd
Y	nd	3.22	3.7	3.71	1.90	1.95	nd	1.03	2.2	2.5	5.34	3.16	17.2	2.16	0.21
Hf	nd	0.05	nd	0.05	0.05	0.07	nd	0.03	0.02	0.03	0.22	0.04	0.63	0.04	0.01
V	—	151.6	435.3	—	82	—	—	45	67	67	72	105	176.9	99	—
Cr	5647	2274	2447	—	1390	—	3447		493.8	489	1828	719	389	—	6629
Ni	1843	607	660	—	733	—	1080	962	139.5	129	680	128	63	98	2230
Co	124.1	54.1	—	91.3	21.6	111.7	113.6	—	37.8	35.9	118.3	34.5	21.8	—	124.7
Pb	0.12	0.08	—	0.15	—	0.49	0.11	—	0.12	0.29	0.90	0.13	4.4	0.60	0.09
U	nd	0.01	nd	0.01	0.12	0.13	nd	0.01	nd	nd	0.09	nd	0.03	0.001	nd
La	0.02	0.08	0.10	0.08	0.17	0.13	0.04	0.07	0.24	0.22	1.59	0.24	1.42	0.07	0.02
Ce	0.06	0.29	0.29	0.28	0.36	0.33	0.14	0.17	0.60	0.54	3.14	0.63	4.23	0.18	0.07
Pr	0.01	0.06	—	0.06	—	0.06	0.02	0.03	0.08	0.08	0.38	0.10	0.78	0.04	0.01
Nd	0.06	0.39	0.33	0.38	0.32	0.23	0.15	0.18	0.38	0.36	1.48	0.48	4.19	0.21	0.04
Sm	0.03	0.20	0.13	0.21	0.15	0.12	0.06	0.07	0.13	0.12	0.38	0.16	1.49	0.12	0.01
Eu	0.01	0.10	0.06	0.10	0.06	0.07	0.04	0.04	0.13	0.09	0.13	0.10	0.59	0.10	0.01
Gd	0.06	0.32	0.26	0.34	0.19	0.18	0.10	0.11	0.19	0.20	0.51	0.26	1.92	0.19	—
Tb	0.01	0.07	—	0.07	—	0.04	0.02	0.02	0.04	0.04	0.10	0.05	0.37	0.05	0.00
Dy	0.08	0.50	0.48	0.52	0.31	0.28	0.14	0.17	0.31	0.34	0.72	0.44	2.5	0.35	0.03
Ho	0.02	0.12	0.12	0.12	—	0.07	0.03	0.04	0.07	0.08	0.17	0.11	0.57	0.09	0.01
Er	0.06	0.34	0.36	0.35	0.22	0.19	0.10	0.11	0.21	0.25	0.52	0.31	1.60	0.27	0.02
Tm	—	—	—	—	—	—	—	—	—	—	—	—	—	0.04	—
Yb	0.07	0.33	0.34	0.34	0.23	0.20	0.10	0.12	0.22	0.24	0.57	0.31	1.56	0.26	0.03
Lu	0.01	0.05	0.05	0.05	0.03	0.03	0.02	0.02	0.03	0.04	0.09	0.05	0.23	0.04	0.01

Table 3 (*concluded*).

Sample:	98SJ2	97SJ6	97SJ8	97SJ8	97SJ10	97SJ10	98SJ4	97SJ33	97SJ1	97SJ3	97SJ4	97SJ9	97SJ13	97SJ40	98SJ3
Name:	Dunite	Wehrlite	Wehrlite*	Duplicate	Wehrlite*	Duplicate	Wehrlite	Wehrlite**	Gabbro	Gabbro	Gabbro	Gabbro	Gabbro	Gabbro**	Ultramafic dyke
$(La/Yb)_n$	0.4	0.48	—	0.47	—	0.66	0.44	0.43	0.74	0.62	1.88	0.52	0.58	0.18	1.21
$(La/Sm)_n$	0.17	0.39	—	0.2	—	0.43	0.28	0.67	1.16	1.15	2.63	0.94	0.55	0.35	0.56

Note: nd, not detected; —, not analysed; *samples analysed at ANU (Canberra, Australia); **samples from Lapierre et al. (2000). Major elements are reported on volatile-free basis. LOI, loss on ignition.

completely removed during mineral separation. Clinopyroxene and amphibole separates from SJ40 gabbro have similar εNd_ivalues of +5 (εNd_i = 5.8 and +5.6, respectively), while the SJ40 plagioclase separates has a lower εNd_i of +4.6.

The wehrlites exhibit a limited range of initial $^{87}Sr/^{86}Sr$ ratios (0.70282–0.703250), except for the plagioclase-rich wehrlite (97SJ6), which has a higher ratio (0.703412). The gabbros exhibit a large range of initial $^{87}Sr/^{86}Sr$ (0.70316–0.704088), which all are higher than those of the peridotites. In the εNd_i–εSr_i diagram (Fig. 8), the San Juan plutonic rocks plot in the oceanic island basalt (OIB) field and within the mantle array (with the exception of 97SJ6 and 97SJ13 plagioclase and amphibole, 97SJ10 clinopyroxene).

Initial lead isotopic compositions of whole rocks and mineral separates from cumulate wehrlites and gabbros are broadly homogeneous (Table 4) and fall in the field of the East Pacific Ridge (EPR) MORB (mid-ocean ridge basalt) in the $^{208}Pb/^{204}Pb$–$^{206}Pb/^{204}Pb$ correlation plot (Fig. 9). The gabbro 97SJ13 and its related plagioclase have the highest $(^{206}Pb/^{204}Pb)_i$ and $(^{208}Pb/^{204}Pb)_i$ ratios, and clinopyroxene separates from the wehrlite 97SJ10 have the lowest (Table 4; Fig. 9). Pb isotope ratios of wehrlites (97SJ8, 98SJ4) and olivine gabbro (98SJ9) are very similar. The San Juan suite domain falls close to the Northern Hemisphere reference line of Zindler and Hart (1986) in the $^{208}Pb/^{204}Pb$–$^{206}Pb/^{204}Pb$ diagram (Fig. 9), but above in the $^{207}Pb/^{204}Pb$–$^{206}Pb/^{204}Pb$ plot, because of the high $(^{207}Pb/^{204}Pb)_i$ of the San Juan suite rocks and minerals. Solely, the isotropic gabbro (97SJ13) falls on the NHRL (Fig. 9). The Lower Cretaceous San Juan whole rocks and mineral separates are less radiogenic in Pb than the volcanic rocks of the Late Cretaceous Caribbean oceanic plateau (refer to the field of the southwest Colombia in Fig. 9; Hauff et al. 2000*a*; Kerr et al. 2002*b*). The high-Mg basalts and ankaramites from the Late Cretaceous Caribbean oceanic plateau are characterized by higher $^{207}Pb/^{204}Pb$ ratios (Fig. 9) (high-U/Pb mantle (HIMU) component; Hauff et al. 2000*a*, 2000*b*; Lapierre et al. 2000; Kerr et al. 2002*b*; Mamberti et al. 2003).

The San Juan cumulates formed from the accumulation of olivine, succeeded by clinopyroxene and plagioclase. Rocks of intermediate to felsic compositions are absent. Orthopyroxene and amphibole are resctricted to the uppermost gabbroic levels. The Nd and Pb ratios, with the exception of the $(^{207}Pb/^{204}Pb)_i$, of the San Juan cumulates fall in the range of within-plate intra-oceanic basalts.

Discussion

In this section we will focus on two questions: (1) the nature of the original magmatic liquids and interpretation of the major- and trace-element compositions of the cumulate rocks and (2) the tectonic setting in which the intrusions were emplaced.

Compositions of original magmatic liquids

All the intrusive rocks of the San Juan suite are cumulates. This complicates the interpretation of their chemical compositions. To infer the nature of the liquids from which they crystallized, we must use a combination of mineral compositions and whole-rock compositions. The major- and incompatible trace-element compositions of the San Juan cumulate

Table 4. Nd, Sr, and Pb isotopic compositions for the San Juan rocks and mineral separates.[a]

A	Sample:	98SJ2	97SJ6	97SJ8	97SJ10	98SJ4	97SJ33	97SJ1	97SJ3	97SJ4
	Name:	Dunite	Wehrlite	Wehrlite	Wehrlite	Wehrlite	Wehrlite**	Gabbro	Gabbro	Gabbro
	$^{87}Rb/^{86}Sr$	0.1041	0.017852	0.025798	0.055086	0.029232	0.021294	0.003451	0.006535	0.274514
	$^{87}Sr/^{86}Sr$	0.704676±20	0.703443±14	0.703295±15	0.703301±21	0.703295±8	0.703448±13	0.703124±8	0.704099±16	0.703941±11
	$(^{87}Sr/^{86}Sr)_i$	0.70449	0.703412	0.70325	0.703205	0.703244	0.70341	0.703844	0.704088	0.703461
	εSr_{123Ma}	2.00	–13.40	–15.70	–16.34	–15.78	–13.41	–7.26	–3.80	–12.7
	$^{147}Sm/^{144}Nd$		0.219259	0.396775	0.283414	0.252258	0.266018	0.357278	0.201538	0.155233
	$^{143}Nd/^{144}Nd$		0.513073±15	0.512981±8	0.513040±9	0.512960±26	0.512822±14	0.513089±5	0.513011±12	0.512871±15
	$(^{143}Nd/^{144}Nd)_i$		0.512897	0.512662	0.512812	0.512757	0.512607	0.512801	0.512848	0.512746
	εNd_{123Ma}		8.13	5.94	6.48	5.41	2.50	6.28	7.18	5.20
	$(^{206}Pb/^{204}Pb)_m$		18.48		18.4					
	$(^{206}Pb/^{204}Pb)_i$		18.42		18.31					
	$(^{206}Pb/^{204}Pb)_i$*		18.4		18.38					
	$(^{207}Pb/^{204}Pb)_m$		15.59		15.53					
	$(^{207}Pb/2^{04}Pb)_i$		15.59		15.53					
	$(^{207}Pb/^{204}Pb)_i$*		15.59		15.53					
	$(^{208}Pb/^{204}Pb)_m$		38.17		38.01					
	$(^{208}Pb/^{204}Pb)_i$		38.16		38					

B	Sample:	97SJ12	98SJ3	98SJ5	97SJ13	97SJ13	97SJ10	97SJ40	97SJ40	97SJ40
	Name:	Dacite	Ultramafite	Dolerite	Amph**	Plag**	Cpx	Plag**	Cpx**	Amph**
	$^{87}Rb/^{86}Sr$		0.10793	0.009214	0.080529	0.014656	0.075576	0.002545	0.002545	0.072188
	$^{87}Sr/^{86}Sr$		0.705305±12	0.703311±8	0.705040±13	0.704646±10	0.705176±12	0.703162±7	0.703588±10	0.703473±20
	$(^{87}Sr/^{86}Sr)_i$		0.70512	0.703295	0.704899	0.70462	0.705043	0.703157	0.703157	0.703335
	$epsSr_{123Ma}$		10.80	–15.06	7.70	3.80	9.80	–17.01	–12.44	–14.33
	$^{147}Sm/^{144}Nd$	0.1557		0.192294	0.236703	0.111721	0.288282	0.131432	0.376794	0.347888
	$^{143}Nd/^{144}Nd$	0.512089±8		0.513051±6	0.513045±4	0.512962±9	0.512860±40	0.512822±18	0.513079±11	0.513046±16
	$(^{143}Nd/^{144}Nd)_i$	0.511964		0.512896	0.512855	0.512872	0.512628	0.512716	0.512776	0.512766
	$epsNd_{123Ma}$	–10.07		8.13	7.31	7.66	2.89	4.62	5.84	5.59
	$(^{206}Pb/^{204}Pb)_m$				18.58	18.28				
	$(^{206}Pb/^{204}Pb)_i$		18.42		18.52	18.17	18.13			
	$(^{206}Pb/^{204}Pb)_i$*				18.56	18.23				
	$(^{207}Pb/^{204}Pb)_m$				15.54	15.53				
	$(^{207}Pb/2^{04}Pb)_i$		15.55		15.53	15.53	15.47			
	$(^{207}Pb/^{204}Pb)_i$*				15.54	15.53				
	$(^{208}Pb/^{204}Pb)_m$				38.17	38				
	$(^{208}Pb/^{204}Pb)_i$		38.17		38.13	37.9	37.89			

Note: subscript m, ratios measured; subscript i, calculated initial ratios based on the U, Th, and Pb contents measured by ICP–MS (refer Table 2);
* indicates initial ratios calculated using the Pb and U abundances determined on the basis the Nb/U and Ce/Pb ratios and assuming that Nb and Ce have not been mobilized (Hofman et al. 1986);
** indicates data after Lapierre et al. 2000. Amph, amphibole; Cpx, clinopyroxene; Plag, plagioclase.
[a]Age of all samples = 123 Ma.

Fig. 4. Rb, Ba, and Sr vs. Ce correlation diagrams of the San Juan peridotites and gabbros. The 2σ error bars of the very low concentrations are included in the symbol sizes.

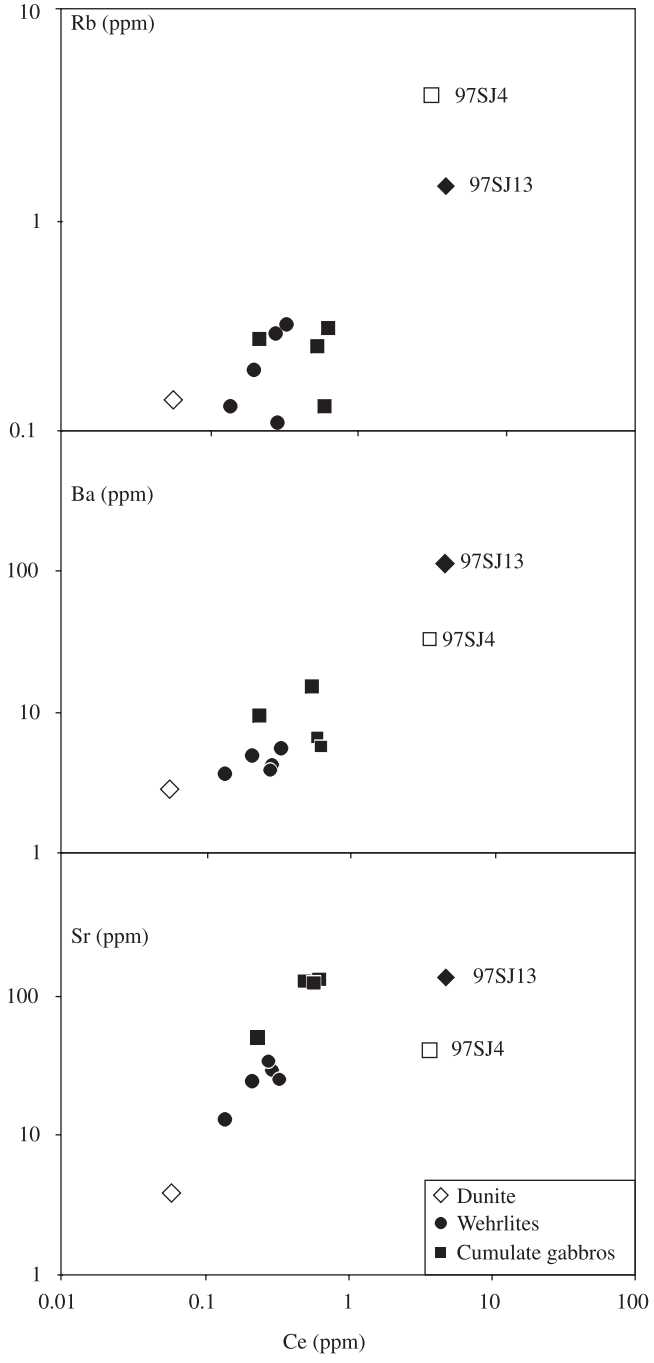

rocks depend both on the nature of the predominant minerals and the partitioning of REE and incompatible trace elements in these minerals.

The composition of the basaltic liquid in equilibrium with the cumulate peridotite and olivine gabbros can be estimated from the forsterite contents of the olivine crystals in these rocks. Révillon et al. (2000) estimated the composition of the parental magmas using curves representing the composition of olivine in equilibrium with liquids with 8%, 9%, and 10% of FeO. The calculations were made using Mg–Fe

Fig. 5. Al_2O_3, CaO, SiO_2, and FeO vs. MgO correlation diagrams of the San Juan peridotites and gabbros. Mineral compositions from Hall (1987). Amph, amphibole; Cpx, clinopyroxene; Opx, orthopyroxene.

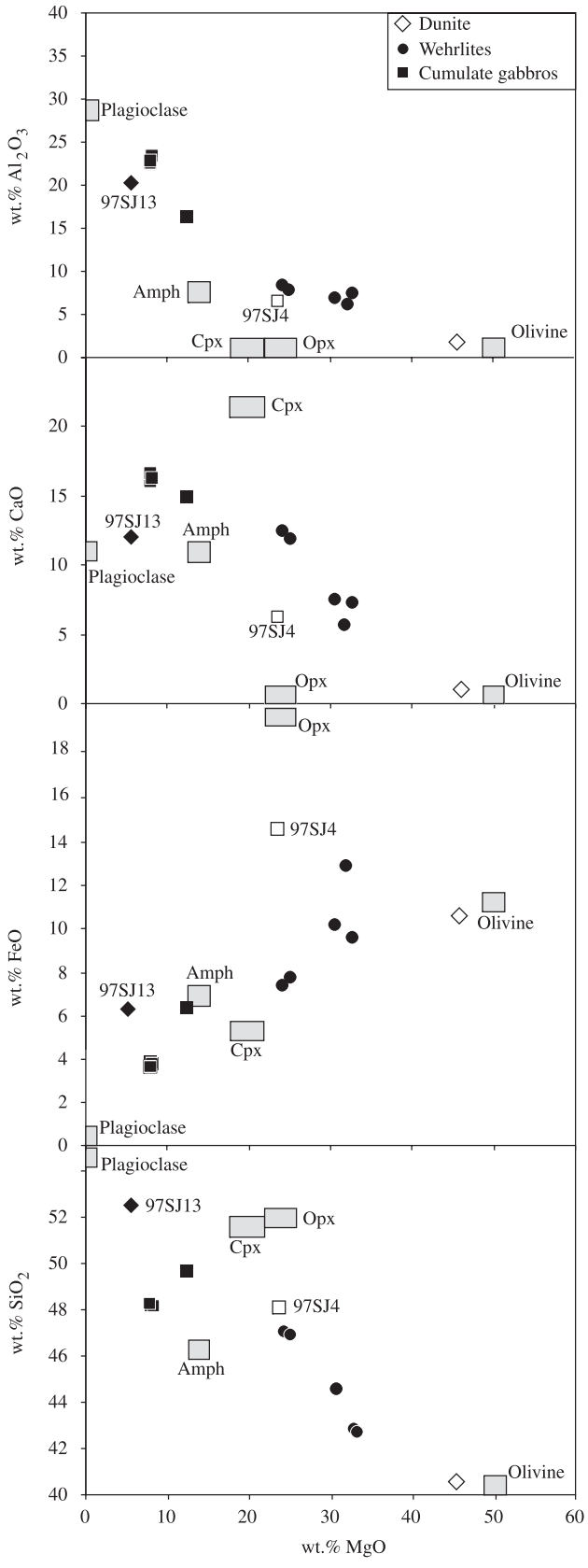

Fig. 6. TiO_2 vs. MgO correlation diagram of the San Juan peridotites and gabbros. On the basis of the major-element chemistry of the plutonic rocks (Table 2) and assuming that the MgO content of the parental liquid is 16% (see the text), this diagram shows that dunites and wehrlites were the first to be formed by olivine accumulation (1), followed by the gabbros related to plagioclase accumulation (2), and the 97SJ13 gabbro, considered as the residual liquid (3).

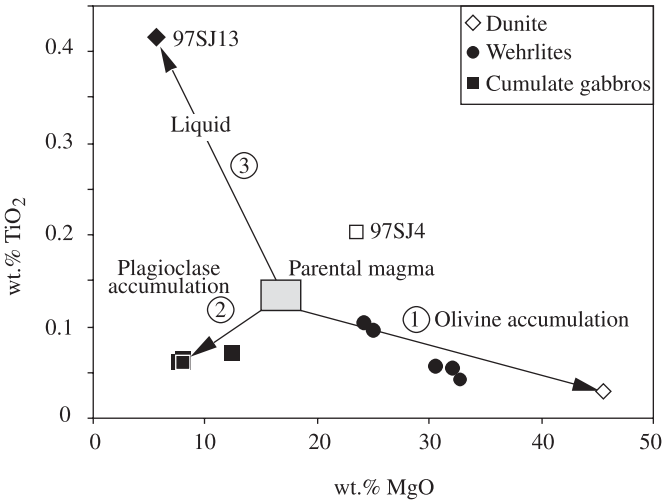

olivine-liquid partition coefficient of 0.3 (Roeder and Emslie 1970). These values correspond to the ferrous oxide content of the inferred parental magmas as estimated from whole-rock composition, assuming ferric iron equals 15% of the total iron content of the magma. If the most magnesian olivine from a sample plots on an olivine-liquid equilibrium curve, this indicates that the MgO content of the whole rock is that of the liquid from which the olivine crystallized; if the olivine plots below the curves, this indicates that the rocks have accumulated olivine. We have used this procedure to estimate the MgO content of the parental magmas of the San Juan dunites, wehrlites, and olivine gabbros. Calculated MgO contents of the San Juan parental magmas range from 16% in the dunites and 8% in the wehrlites to 2% in some gabbros.

To determine the REE compositions and Nb abundances in melts in equilibrium with clinopyroxene, we used the partition coefficients of Hart and Dunn (1993). The calculated melts are compared with the composition of the Piñon dolerites that have been interpreted to represent the uppermost levels of the Lower Cretaceous oceanic plateau (Reynaud et al. 1999; Lapierre et al. 2000). As seen in Fig. 10, the calculated melts have flat HREE patterns with abundances similar to or lower than those of the mafic rocks. The LREE are slightly enriched. The La/Nb ratios of the melts in equilibrium with clinopyroxene separates from the wehrlites, cumulate, and isotropic gabbro ranges from 0.44 to 1.64.

Before trying to explain the trace-element distribution in the San Juan cumulates, we must first estimate the abundance of trapped liquid in these rocks. It is possible to do this using the measured compositions and modal abundances of the cumulus minerals and by making an assumption about the composition of the trapped liquid. On the basis of the major-element chemistry of the San Juan plutonic rocks (Table 2) and assuming that the MgO content of the parental magma is 16%, TiO_2–MgO plot (Fig. 6) shows that dunites and wehrlites were the first to be formed by olivine accumulation (1), followed by the gabbros related to plagioclase accumulation (2), and the residual liquid (3), represented by the SJ13 isotropic gabbro, ascent to the surface. On the basis of the Nd content of the SJ13 isotropic gabbro, considered as the residual liquid and using the mass balance of the cumulates (gabbros and wehrlites), we can estimate the abundance of trapped liquid in these rocks using the calculation described in Appendix A. The results of these calculations (see Appendix A) show that the abundances of trapped liquid in the cumulate rocks range between 5% (97SJ10 wehrlite) and 2% (97SJ3 gabbro).

The relative concentrations of trace elements, such as the REE, Nb, and Zr, in the cumulates will depend on the proportion of trapped liquid and the nature of the cumulus minerals. Their overall levels will be controlled mainly by the relative proportions of minerals, such as olivine and plagioclase, with which these elements are incompatible, and the amount of trapped liquid. The relative abundances, on the other hand, will be influenced by the amount of clinopyroxene, a mineral for which the partition coefficients vary significantly. As is well known, the HREE are far more compatible in clinopyroxene than the LREE; what is less appreciated is that Nb and Zr are significantly less compatible than the REE. The mantle-normalized trace-element pattern of a clinopyroxene-rich cumulate is, therefore, characterized by negative anomalies for these elements.

These effects are illustrated by the trace-element composition of the wehrlite 97SJ10, which contains about 20 modal% of clinopyroxene and 70% of olivine. We estimate that this sample contained about 5% trapped liquid. It is seen in Fig. 7 that the clinopyroxene and whole rock have similar LREE-depleted patterns but that REE abundances in the whole rock are lower than in the clinopyroxene. The differences in abundances are explained by the relatively small amount of the trapped liquid and the high proportion of olivine, which contains no REE and lowers concentrations in the cumulate rock. The marked negative Nb and Zr anomalies in both the clinopyroxene and whole rock can be explained in the same way. Both elements are less compatible than the REE and are present in very low concentrations in the clinopyroxene, which controls the composition of the cumulate.

The trace-element chemistry of the cumulate gabbros depends on the relative abundances of plagioclase and clinopyroxene. Because the LREE are more compatible than the HREE in plagioclase, a cumulus gabbro rich in this mineral will have a relatively flat REE pattern. This is seen in the samples 97SJ1, 97SJ3, and 97SJ9, which are characterized by flat REE patterns. The compatible nature in plagioclase of Eu and Sr results in marked positive anomalies for these elements.

Criteria that discriminate between gabbroic intrusions in oceanic plateaus, normal oceanic crust, and island arcs

The geodynamic environment in which cumulate intrusive rocks are emplaced is difficult to establish when spatial relations with cogenetic basalts are obscured by later tectonic events. In such cases, it is unclear whether an intrusion was once part of normal oceanic crust, or part of an oceanic pla-

Fig. 7. Chondrite- and primitive mantle-normalized (Sun and McDonough 1989) rare-earth element patterns and multi-element plots for peridotites, gabbros, ultramafic dyke, and mineral separates of the San Juan sequence. amph, amphibole; cpx, clinopyroxene; plag, plagioclase.

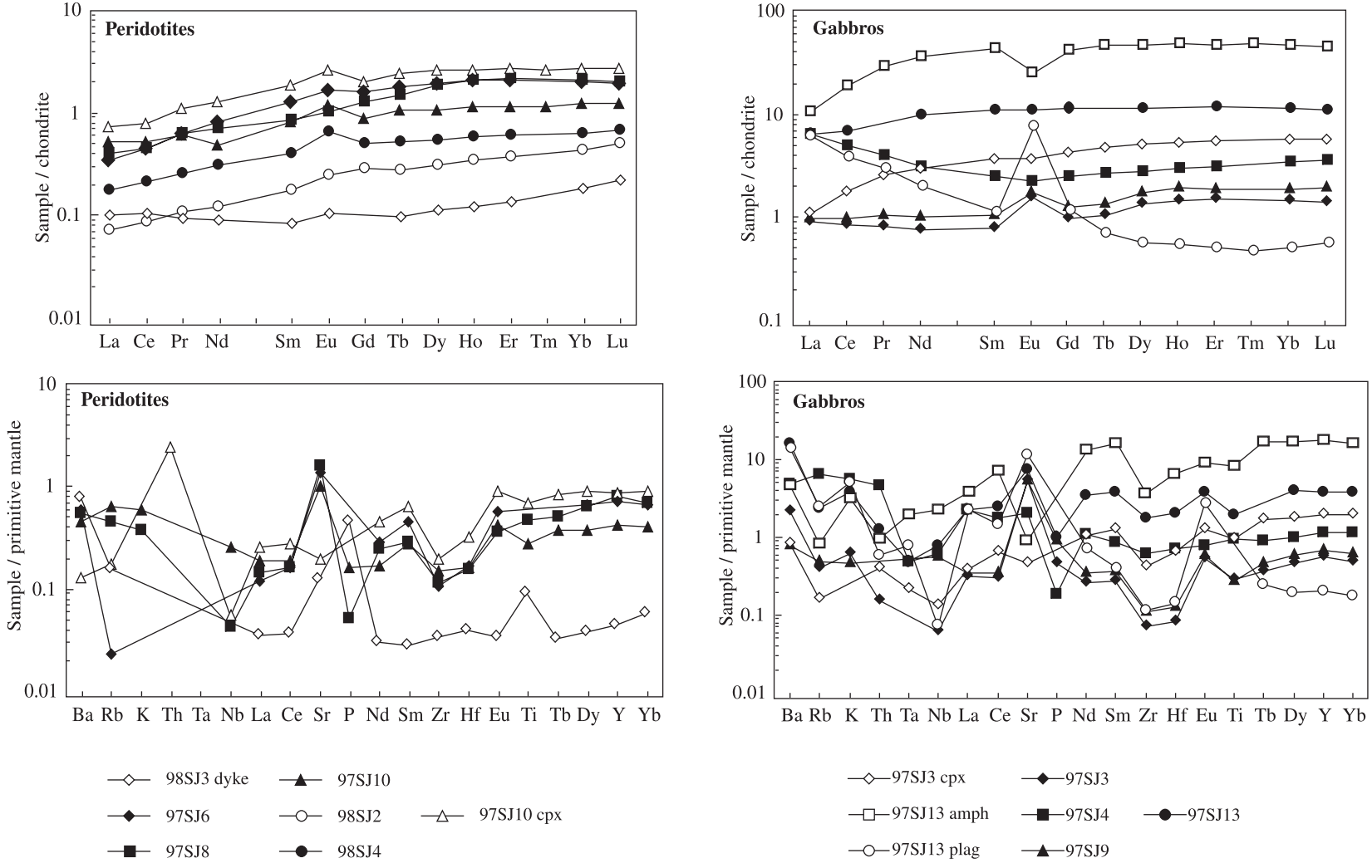

Fig. 8. εNd_i–εSr_i correlation diagram of the San Juan plutonic rocks. The oceanic island basalt (OIB) field is after DePaolo (1988). MORB, mid-oceanic ridge basalt; amph, amphibole; cpx, clinopyroxene; plag, plagioclase.

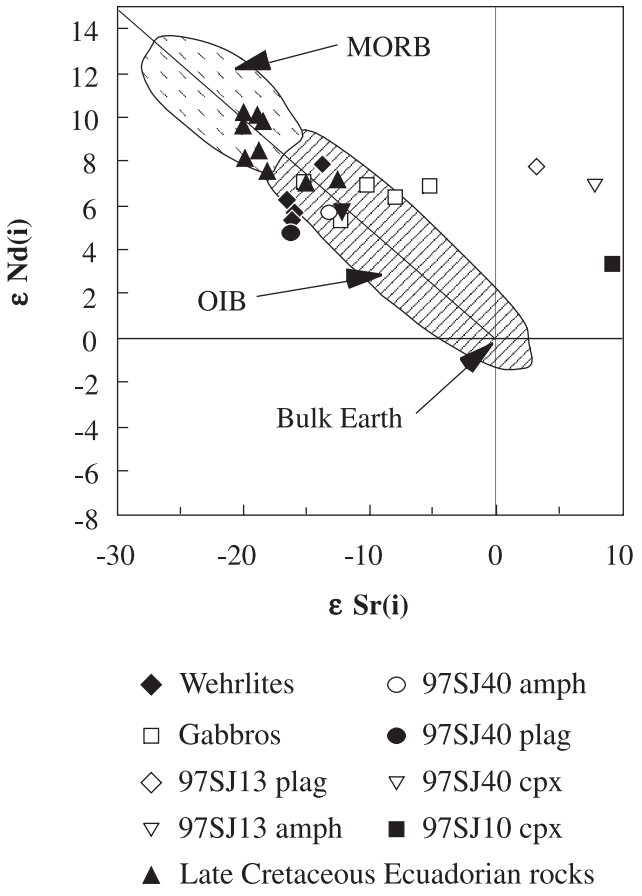

teau, or related to subduction magmatism. To distinguish among these possibilities, we need to develop criteria to establish the tectonic setting in which the intrusions were emplaced.

There are three broad types of criteria: (1) geodynamic setting and broad lithological associations; (2) mineralogy and major-element compositions; (3) trace-element and Sr, Nd, Pb isotope compositions.

Geodynamic setting and lithological associations

Even in cases in which the tectonic setting is obscured by later events, it is often possible to gain some insights from structural relationships and the identification of diagnostic lithological associations. For example, oceanic ridges and plateaus are made up dominantly of monotonous, commonly pillowed tholeiitic basalts associated with pelagic sediment, whereas subduction-related units contain more diverse calc-alkaline rocks whose compositions range from basalt to rhyolite. Tephras layers are rare in oceanic plateau, while they are very common in arc settings. Occurrence of high-MgO basalts and the apparent absence of sheeted dyke complexes represent discriminant features of oceanic plateaus (Kerr et al. 2000).

Magma compositions and crystallization sequences

The parental magmas of volcanic and intrusive rocks from different settings differ significantly in composition because of differences in the nature of their sources and conditions of melting. The magma erupted at mid-ocean ridges is essentially anhydrous. Because of the absence of lithosphere beneath the ridge, the degree of melting is relatively high and melting takes place at a relatively shallow depth. Under these conditions, the aluminous phase (plagioclase) is unstable and totally enters the melt. The resultant magma is rich in Al, with relative low Fe and Na and relatively high Mg. This type of magma will crystallize olivine first (like any melt produced by melting of peridotite) and this phase will be joined early in the crystallization sequence by plagioclase. The expected crystallization sequence is olivine (ol) → plagioclase (plag) → clinopyroxene (cpx) → orthopyroxene (opx). The first two phases are those commonly observed as phenocrysts in mid-ocean ridge basalts (Wilson 1989; Juteau and Maury 1997).

The parental magma of an oceanic island or oceanic plateau forms at greater depth because the melting takes place beneath the oceanic lithosphere. This magma may be poorer in Al because this element is partially retained in aluminous ortho- or clinopyroxene. It is richer in Fe because of the higher pressure and in Na because of lower degree of partial melting. The second silicate phase to crystallize (after olivine) is clinopyroxene, and plagioclase crystallizes relatively late. The expected sequence is chromite → ol → cpx → plag → (opx), as could be inferred from the phenocryst assemblage in oceanic island basalts (Wilson 1989; Juteau and Maury 1997).

The parental magma of oceanic island-arc magma forms in the presence of water ± other volatiles. This changes the relative stabilities of the major phases, reducing the stability of olivine relative to plagioclase, clinopyroxene, and orthopyroxene. During crystallization, olivine is joined early by clinopyroxene, orthopyroxene, and plagioclase, and Fe–Ti oxides are early and abundant. Plagioclase is usually the most abundant phenocryst phase and generally displays complex oscillatory zoning with Ca-rich cores. It is characteristically highly calcic but shows a wide range of compositions within each of the major magma series. The high Ca contents have been attributed to the high water contents of island-arc magmas. Orthopyroxene is a common phenocryst phase but does not occur with olivine or amphibole. The expected sequence is (chromite) ol → anorthite → Fe–Ti oxide → plag ± opx ± cpx → hydrous minerals. Again, this sequence can be confirmed from phenocryst assemblages in volcanic rocks from island arcs (Juteau and Maury 1997).

Trace-element and isotope characteristics

The source of mid-ocean ridge basalts is depleted both in terms of trace elements and isotopic ratios. The degree of partial melting is high and the only residual phases are olivine and orthopyroxene (Juteau and Maury 1997). Normal MORBs are depleted in LREE and other incompatible elements, and their Nd isotope ratios are very high (εNd_i = +10 to +12).

Basalts of oceanic islands and plateaus form at greater depth from generally less homogeneous sources than MORB. During the melting that forms oceanic island basalts, clinopyroxene ± garnet are residual, and the magma becomes strongly enriched in incompatible trace elements relative to the source. REE patterns are flat to light REE

Fig. 9. ($^{208}Pb/^{204}Pb)_i$ vs. ($^{206}Pb/^{204}Pb)_i$ and ($^{207}Pb/^{204}Pb)_i$ vs. ($^{206}Pb/^{204}Pb)_i$ diagrams for peridotites, gabbros, and mineral separates from the San Juan sequence. Basalts and dolerites from the Piñon Formation are reported after Reynaud et al. (1999) and Lapierre et al. (2000). Pb isotopic compositions of the Ecuadorian Lower Cretaceous plutonic and volcanic rocks fall in the common field of the East Pacific Rise MORB and the Late Cretaceous Ecuadorian Rocks belonging to the Cretaceous Caribbean–Colombian Oceanic Plateau (CCOP) (Mamberti et al. 2003). The Northern Hemisphere reference line (NHRL) and the field from some mantle reservoirs are reported after Zindler and Hart (1986). East Pacific Ridge (EPR) MORB and Mid-Atlantic Ridge (MAR) MORB data and Galapagos Islands field are from White et al. (1987). The southwestern Colombia field, which consists of Upper Cretaceous high-MgO basalts and picrites, is reported after Hauff et al. (2000*b*) and Kerr et al. (2002*b*). The Late Cretaceous Ecuadorian rocks are from Mamberti et al. (2003). DMM, depleted MORB mantle; EM1, enriched mantle 1; EM2, enriched mantle 2; HIMU, high-U/Pb mantle.

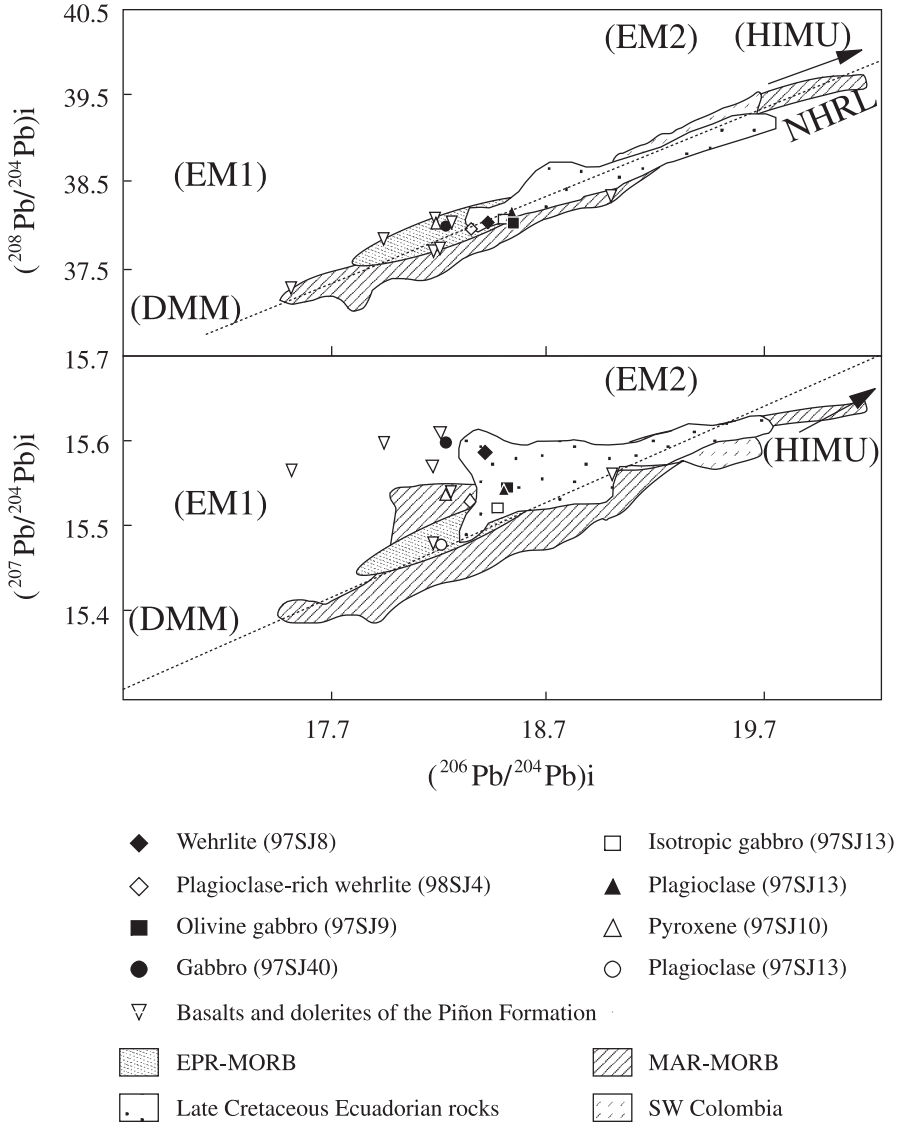

enriched, depending on the nature of the source and the extent of melting. Basalts in oceanic plateaus generally have flat REE patterns but the most Mg-rich melts (picrites and komatiites) may be enriched or depleted in LREE (Kerr et al. 1998). The Nd isotopic compositions of OIB span a very large range of values (+9 to –6) from moderately depleted to strongly enriched, in contrast to the compositions of basalts from oceanic plateaus which are more uniform and only slightly less depleted than MORB.

Arc basalts come from sources with distinctive characteristics. Their REE patterns vary from enriched to depleted LREE compared with heavy REE and mantle-normalized plots that display characteristic negative Nb and Ta anomalies. These anomalies are absent in N-MORB (normal MORB) and plume-related basalts. The Nd isotope compositions of arc basalts are similar to those of OIB.

Test cases

Before using the above criteria to evaluate the geologic setting of the San Juan suite, we will test them against the characteristics of several intrusions for which the tectonic setting is well known.

Intrusions at mid-ocean ridges

Because of their inaccessibility, very few studies of intrusions at mid-ocean ridges have been undertaken. Until 1975,

Fig. 10. Chondrite-normalized REE patterns of calculated melts from the clinopyroxene of San Juan wehrlite and olivine gabbro. These calculated melts are compared with dolerites (97MA18) and isotropic gabbro (97M5). Fm, Formation.

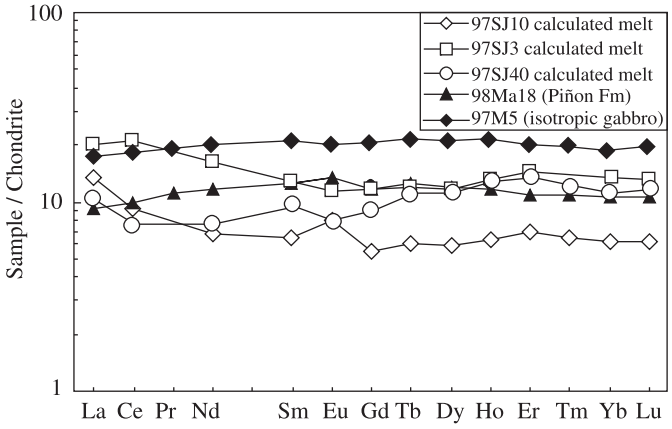

Fig. 11. Primitive mantle normalized (Sun and McDonough 1989) multi-element plots showing the compositional range of olivine gabbros from Ecuador (this study) compared with those from the Southeast Indian Ridge (Hart et al. 1999; Coogan et al. 2001). Note that gabbros from both Indian and Atlantic mid-oceanic ridges share a negative Nb anomaly in common with the San Juan gabbros.

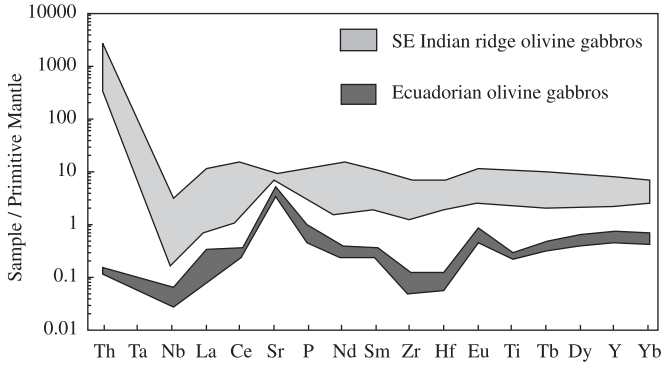

the only available plutonic samples were collected during dredging. More recently, drilling and submersible sampling of cliffs along transform faults has yielded samples of mafic cumulates and higher level gabbros from three main regions: the MARK area on the Mid-Atlantic Ridge (Cannat et al. 1995; Casey 1997; Kempton and Hunter 1997; Coogan et al. 2000), Hess Deep in the eastern Pacific Ocean (Francheteau et al. 1990, 1992; Pedersen et al. 1996), and site 735B of Ocean Drilling Program (ODP) leg 118 in the Indian Ocean (Dick et al. 1991; Hart et al. 1999; Coogan et al. 2001).

The predominant rocks from both areas are gabbros, norites, and troctolites, in which clinopyroxene and plagioclase are cumulus phases and olivine is an interstitial phase. The lower portions of some sections contain serpentinized peridotites and cumulate gabbros.

The gabbroic rocks exhibit a large range of REE patterns. Some are strongly depleted in LREE, others are slightly enriched in these elements. They systematically exhibit a negative Nb anomaly (Fig. 11; Hart et al. 1999; Coogan et al. 2001). Clinopyroxenes separated from the gabbros have a narrow range in REE contents (Gillis 1996; Coogan et al. 2000) and are depleted in LREE with a negative Eu anomaly. The $^{143}Nd/^{144}Nd$ ratios of the gabbros have values typical of MORB (Pedersen et al. 1996; Hart et al. 1999).

Ophiolites

Complete sections through oceanic crust, as exposed in well-known ophiolites such as Cyprus, Newfoundland, Josephine, and Coast Range ophiolites, are now thought to represent remnants of back-arc basins (Pearce et al. 1984; Shervais 2001). The principal arguments are the identification of geochemical features typical of subduction-related rocks, such as low TiO_2 contents (<1.5%; Miyashiro 1973) and negative Nb anomalies (Saunders et al. 1980; Jenner et al. 1991). In contrast, the ophiolites of Oman have been interpreted as coming from true oceanic crust (Juteau et al. 1988; Nicolas et al. 1988).

The cumulate sections of the Maqsad massif in the Oman ophiolite (Benoit et al. 1996; Benoit 1997) consist of troctolites, olivine gabbros, norites, pyroxenites, and dunites. These rocks are generally similar to those of ocean ridges but are characterized by a greater abundance of orthopyroxene in both the gabbroic and ultramafic sections and by the presence of brown (magmatic) amphibole in the uppermost gabbroic levels. The crystal sequence in the ultramafic cumulates is ol → cpx → plag ± opx.

Rare-earth element patterns range from flat to depleted, with or without Eu anomalies. All the cumulate rocks exhibit negative Nb and Zr anomalies of variable magnitude. The εNd_i values of the intrusive rocks range from +6 to +10. Two types of basaltic units separated by an unconformity have been distinguished in the Oman ophiolite. The lower unit display N-MORB affinities, while the upper one is characterized by negative Nb anomalies, characteristic features of arc tholeiites (Pallister 1984). Negative Nb and Zr anomalies in the cumulate rocks are absent in the N-MORB-type lower unit that immediately overlies the plutonic sections. This lower basaltic unit is interpreted as cogenetic with the intrusive cumulate rocks and developed along a fast spreading ridge. The upper unit is interpreted as developed in an intra-oceanic arc setting. Thus, the negative Nb anomalies observed in the Oman cumulate rocks are probably due to fractionation during clinopyroxene accumulation.

Intrusions in oceanic islands

Few samples of intrusions in oceanic islands are available, and most of those that exist are from intrusions with a clearly alkalic character that is very different from the magmas that fed oceanic plateaus. One source of information comes from suites of xenoliths found in alkaline volcanic rocks on islands, such as Hawaii and Kerguelen (Grégoire et al. 1998). Xenoliths believed to come from the lower crust contain plagioclase- or spinel-rich assemblages and Fe-rich mafic minerals. In such suites, the mineral assemblages are olivine, clinopyroxene, orthopyroxene, plagioclase, spinel, and Fe–Ti oxides. Crystallization sequences include ol → spinel → cpx → opx → plag in the ultramafic rocks and spinel → cpx → opx → plag in the gabbros. Intrusions of tholeiitic character in the Kerguelen Archipelago consist of gabbros and olivine, clinopyroxene, and plagioclase cumulates (Giret and Beaux 1984).

Ultramafic to mafic xenoliths from Kerguelen display low REE abundances at near chondritic values. Their normalized

patterns are usually flat, but rare examples are either slightly LREE-enriched or LREE-depleted. They are interpreted as cumulates of the Kerguelen tholeiitic-transitional basaltic series. Clinopyroxenites and metagabbroic xenoliths have higher REE concentrations and display convex-upward REE, a feature that was attributed by Grégoire et al. (1998) to metasomatic enrichment in the middle REE patterns. These xenoliths represent high-pressure cumulates of alkaline magmas produced during the recent phase activities of the Kerguelen plume. The εNd_i values of these xenoliths span a large range, from + 4 to –2 (Vance et al. 1989; Mattielli 1996).

Intrusion in an oceanic island arc, the Chilas complex from Kohistan (Himalayas)

The Chilas complex (Pakistan, Himalayas) is interpreted as the plutonic part of a Cretaceous oceanic arc (Bard 1983; Khan et al. 1989, 1993). The volcanic sequence is typical of an island arc comprising basalt, andesite, dacite, and rhyolite of arc-tholeiitic affinity intruded by numerous large to small gabbroic to granitic plutons (Collins et al. 1998). The Chilas intrusive complex itself comprises two distinct rock associations: the gabbroic Main Facies Zone, and the ultramafic–mafic–anorthosite cumulate association.

The Main Facies Zone, which forms at least 85% of the complex, consists of diverse rock types — gabbro (50%–55%), diorite (40%–45%) and minor granite. In the gabbronorites, cumulus orthopyroxene is ubiquitous and abundant (20%–30%), olivine is absent, hornblende is always present in minor quantities, and magnetite forms 2%–4% of the rock. The Main Facies Zone rocks display remarkably uniform and distinctive trace-element patterns. The LREE are slightly enriched, negative Nb anomalies are ubiquitous, and Ba, Rb, K, and Th are strongly enriched relative to the less incompatible elements (Kausar 1998). The εNd_i values are uniform and relatively low (+2.8 to +2.9) (Khan et al. 1993).

The ultramafic–mafic–anorthosite association is composed of cycles of layered to massive olivine, orthopyroxene, clinopyroxene ± plagioclase cumulates. All ultramafic samples are very poor in incompatible elements and the abundances of Rb, Ba, Th, and Nb are below detection limits. Wehrlites are characterized by depletion of LREE, but gabbros have generally flat REE patterns with positive Eu, Ba, and Rb anomalies and negative Nb anomalies in mantle-normalized trace-element plots. The εNd_i values of the cumulate ultramafic and mafic rocks are slightly higher than in the gabbronorites (+3.5 to +4).

Conclusion

On the basis of this review, we conclude that the best criteria to identify the tectonic setting of mafic–ultramafic intrusions are the broad lithological associations and the mineralogy of the cumulus sequences. The presence of abundant calc-alkaline intermediate to felsic rocks clearly identifies an arc setting, such rocks being rare or absent in the oceanic environments. Orthopyroxene is the key diagnostic mineral, being abundant in cumulates from island arcs, present in minor quantities in oceanic crust and ophiolites, but rare to absent from oceanic intraplate magmatism. In places where this mineral is reported, as in the xenolith suites from the Kerguelen Archipelago, it is associated with spinel and other high-pressure phases. Its presence there may indicate crystallization in the lower parts of the volcanic pile (Grégoire et al. 1998). Hydrous minerals are also characteristic of arc-related rocks, but magmatic amphibole is also present in evolved late-stage rocks in ophiolites and oceanic islands.

Also useful are trace-element and Sr, Nd, and Pb isotope compositions, but their interpretation is not always unambiguous. Neodymium isotope ratios of intraplate volcanics are lower than those of mid-ocean ridge basalts, but similar to arc basalts (Sr isotopes are not readily applicable to variably altered rocks). The interpretation of trace-element data is complicated by the accumulation process. A plagioclase cumulate has a flatter REE pattern than the magma from which it crystallizes and is characterized by positive Ba, Sr, and Eu anomalies. A clinopyroxene cumulate has a more depleted pattern and negative Nb and Ta anomalies. Fractionation of Nb (and geochemically similar Ta) from other incompatible elements is particularly important because this process influences the interpretation of negative Nb anomalies, normally a clear signature of a subduction setting. Because Nb is less compatible in pyroxene than the LREE and Th ($Kd_{Nb}^{cpx\text{-}liq}$ = 0.0077 cf. $Kd_{La}^{cpx\text{-}liq}$ = 0.0536; Kd, partion coefficient; Hart and Dunn 1993), a pyroxene cumulate may show negative anomalies that were not present in the host magma. These effects must be taken into account during the interpretation of the trace-element patterns of mafic and ultramafic cumulates.

Plutonic rocks from the Caribbean and Ontong Java plateaus

There is little doubt about the tectonic setting of the ultramafic cumulates and mafic intrusions exposed on Gorgona Island (Echeverria 1980). These rocks share the distinctive geochemical and isotopic characteristics of associated mafic and ultramafic lavas, such as strong depletion of incompatible elements and moderate to high εNd_i values (Révillon et al. 2000). In contrast to the San Juan and mid-ridge oceanic gabbros, they do not have the negative Nb anomaly (Fig. 12). The majority of the intrusive rocks are olivine, clinopyroxene, and plagioclase orthocumulates. Orthopyroxene is absent. On the basis of distinctive textures thought to indicate relatively rapid cooling (abundant small olivine crystals and rare grains with skeletal habits), Révillon et al. (2000) concluded that the intrusions were emplaced at high levels of the Caribbean oceanic plateau.

Gabbros from Santa Isabel (Central province, Solomon Islands) are associated with thin fault-bounded slices of upper mantle peridotite and pillow basalts that are thought to form part of the Ontong Java oceanic plateau (Parkinson et al. 1996). The mafic rocks range in composition from troctolite through olivine gabbro to two-pyroxene gabbro. Magmatic amphibole has never been described in these gabbros. All these gabbros exhibit negative Nb anomalies. The REE patterns range from strongly LREE-depleted to LREE-enriched, and their εNd_i values range from +5.7 to +7.8. On the basis of these results, the setting is ambiguous.

Criteria that demonstrate that the San Juan sequence belongs to an oceanic plateau

Geodynamic setting and broad lithological associations

The supracrustal sequences of the Western Cordillera and along the Pacific coast (Piñon Formation) consist of mafic

Fig. 12. Primitive mantle-normalized (Sun and McDonough 1989) multi-element plots showing the compositional range of isotropic and layered gabbros, and dunites and wehrlites from Ecuador (this study) compared with the dunites, wehrlites, and gabbros from Gorgona Island (Révillon 1999; Révillon et al. 2000).

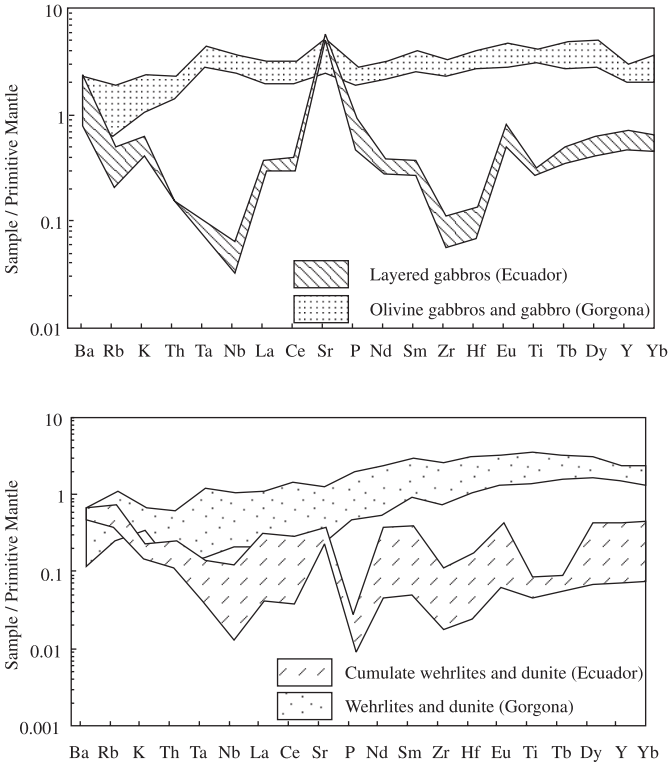

volcanic and hypabyssal rocks, intercalated with pelagic sediments devoid of any interlayered pyroclastic and volcaniclastic rocks. Pyroclastic and volcaniclastic deposits are systematically associated with island-arc basalts and do not occur with plume-derived basalts (Campbell 2001). Evolved calc-alkaline suites of basalt, andesite, dacite, and rhyolite are absent. The San Juan cumulate sequence is not intruded by swarms of basaltic dykes or sheeted dykes, which are common in ophiolites and arc suites.

Magma compositions, mineral assemblages, and crystallization sequences

Plume-related magmas can be Mg-rich. This is a feature of the San Juan sequence. We have shown in a previous section that the MgO content of the basaltic liquids in equilibrium with the ultramafic cumulates ranges from 16% to 8%. Furthermore mineralogy and the crystallization sequence (e.g., chromite → ol → cpx → plag → opx → amphibole) of the San Juan cumulate ultramafic and mafic rocks are similar to those of intraplate volcanic rocks. Orthopyroxene is only a very minor component in the San Juan gabbros, and the ultramafic cumulates are dominated by olivine and clinopyroxene. Amphibole is restricted to the uppermost massive gabbro.

Trace-element and isotopic compositions

The relatively flat REE patterns are typical of rocks from oceanic plateaus and distinct from the depleted patterns of MORB and the more enriched patterns of oceanic island and calc-alkaline arc basalts. The calculated liquid in equilibrium with the clinopyroxene from the wehrlites and gabbros does not show the negative Nb–Ta anomalies present in the cumulate rocks. The trace-element anomalies measured in some samples are either a result of alteration or a feature related to the accumulated minerals. Thus, the negative Nb–Ta anomalies, which are present in the ultramafic rocks but not in the basalts, are related to the accumulation of clinopyroxene and do not indicate a subduction setting.

Nd isotope compositions are not very discriminant because the Nd isotope compositions of oceanic plateau basalts generally overlap those of recent Pacific MORB, ophiolites and arc rocks. However, the majority of the oceanic plateau basalts have εNd_i values ranging between +7 and +9 (Kerr et al. 2000). The εNd_i values of the San Juan plutonic rocks and mineral separates range between +6 and +8, with the exception of 97SJ33 wehrlite and 97SJ10 clinopyroxene separates. Thus, the εNd_i values of the San Juan plutonic rocks and mineral separates fall in the range of the oceanic plateau basalts.

Sr isotopic data are not meaningful in the San Juan plutonic rocks because alteration has modified their $(^{87}Sr/^{86}Sr)_i$ ratio. However, Fig. 9 shows that the San Juan plutonic rocks and mineral separates lie along a mixing line between the depleted mantle (N-MORB) and enriched-plume end members. The enriched end member (EM1) is characterized by high $(^{207}Pb/^{204}Pb)_i$ ratios and could reflect a contamination by recycled lower continental crust or pelagic sediments and (or) altered oceanic crust (EM1). The basalts and dolerites of the Cretaceous Piñon Formation from Ecuador exhibit oceanic plateau affinity and share with the San Juan plutonic rocks more or less similar Pb isotopic ratios and εNd values (with the exception of one basalt with a very low $(^{208}Pb/^{204}Pb)_i$ value and high εNd value, which falls near the depleted mantle (Fig. 9; Reynaud et al. 1999; Lapierre et al. 2000). The Nd and Pb isotopic compositions of both the San Juan plutonic suite and the Piñon volcanic rocks suggest that both suites derived from the mixing of two mantle sources, a depleted MORB-like source and an enriched one.

Summary

A set of criteria has been developed to establish the tectonic setting of mafic–ultramafic intrusions and to identify intrusions that form parts of an oceanic plateau. The more important criteria are the broad lithological associations and the mineralogy of the cumulus sequences.

Mafic and ultramafic volcanic and intrusive rocks exposed in the high parts of the Western Cordillera of Ecuador are shown, using these criteria, to represent different levels of an oceanic plateau. The diagnostic features are the absence of evolved calc-alkaline suites, the crystallization sequence of the cumulate rocks that is similar to that of intraplate rocks, and the presence of basalts with flat REE patterns.

Negative Nb and Zr anomalies in clinopyroxene and host peridotites and gabbros are believed to result from the exclusion of these elements from the structure of cumulus clinopyroxene. They do not indicate a subduction environment.

Acknowledgments

We would like to thank N.T. Arndt for his very helpful comments and for all the time he spent in correcting the manuscript. We are grateful to A.C. Kerr, P.T. Robinson, A.D. Saunders, I.J. Parkinson, S. Goldstein, and M. Wilson for their helpful comments and improving the manuscript. This research has been supported by grants from INSU-CNRS (Intérieur de la Terre, Institut National des Sciences de l'Univers - Centre National de la Recherche Scientifique, France) and FNRS (grant No. 20-50812.97) to M. Polvé and J. Hernandez, respectively. Thanks to Pierre Brunet who did all the Sr-Nd TIMS analyses and to François Sénebier who did all the mineral separates.

References

Aspden, J.A., and Litherland, M. 1992. The geology and Mesozoic collisional history of the Cordillera Real, Ecuador. Tectonophysics, **205**: 187–204.

Bard, J.P. 1983. Metamorphism of an obducted island arc; example of the Kohistan Sequence (Pakistan) in the Himalayan collided range. Earth and Planetary Science Letters, **65**: 133–144.

Barrat, J.-A., Keller, F., Amossé, J., Taylor, R.N., Nesbitt, R.W., and Hirata, T. 1996. Determination of rare earth elements in sixteen silicate reference samples by ICP–MS using a Tm addition and an ion-exchange chromatography procedure. Geostandard Newsletter, **20**: 133–139.

Benoit, M. 1997. Caractérisation Géochimique (traces, isotopes) d'un système de drainage magmatique fossile dans l'ophiolite d'Oman. Unpublished Doctorate thesis in Geochemistry, Université Paul Sabatier, France.

Benoit, M., Polvé, M., and Ceuleneer, G. 1996. Trace element and isotopic characterization of mafic cumulates in a fossil mantle diapir (Oman ophiolite). Chemical Geology, **134**: 199–214.

Campbell, I.H. 2001. Identification of ancient mantle plumes. *In* Mantle plumes: their identification through time. *Edited by* R.E. Ernst and K.L. Buchan. Geological Society of America, Boulder, Colo., Special Paper 352, pp. 5–21.

Cannat, M., Karson, J.A., Miller, D.J., Agar, S.M., Barling, J., Casey, J.F., Ceuleneer, G., Dilek, Y., Fletcher, J., Fujibayashi, N., Gaggero, L., Gee, J.S., Hurst, S.D., Kelley, D.S., Kempton, P.D., Lawrence, R.M., Marchig, V., Mutter, C., Niida, K., Rodway, K., Ross, D.K., Stephens, C., Werner, C.D., and Whitechurch, H. 1995. Site 923: Proceedings of the Ocean Drilling Program, Part A, Initial Reports, Leg 153, pp. 217–258.

Casey, J.F. 1997. Comparison of major- and trace-element geochemistry of abyssal peridotites and mafic plutonic rocks with basalts from the MARK region of the Mid-Atlantic ridge. Ocean Drilling Program, Leg 153, pp. 181–241.

Coffin, M.F., and Eldholm, O. 1993. Scratching the surface; estimating dimensions of large igneous provinces. Geology, **21**: 515–518.

Collins, A.S., Khan, M.A., Stern, R.J., Gribble, R.F., and Windley, B.F. 1998. Geochemical and isotopic constraints on subduction polarity, magma sources and palaeogeography of the Kohistan Arc, northern Pakistan; discussion and reply. Journal of the Geological Society (of London), **155**: 893–895.

Coogan, L.A., Kempton, P.D., Saunders, A.D., and Norry, M.J. 2000. Melt aggregation within the crust beneath the Mid-Atlantic Ridge: evidence from plagioclase and clinopyroxene major and trace element compositions. Earth and Planetary Science Letters, **176**: 245–257.

Coogan, L.A., MacLeod, C.J., Dick, H.J.B., Edwards, S.J., Kwassnes, A., Natland, J.H., Robinson, P.T., Thompson, G., and O'Hara, M. J. 2001. Whole rock geochemistry of gabbros from the Southwest Indian Ridge: constraints on geochemical fractionations between the upper and lower oceanic crust and magma chamber processes at (very) slow-spreadind ridges. Chemical Geology, **178**: 1–22.

Cosma, L., Lapierre, H., Jaillard, E., Laubacher, G., Bosch, D., Desmet, A., Mamberti, M., and Gabriele, P. 1998. Pétrographie et géochimie des unités magmatiques de la Cordillère occidentale d'Equateur (0 degrees 30′); implications tectoniques. Bulletin de la Société géologique de France, **169**: 739–751.

Dalrymple, G.B., Alexander, E.C., Lanphere, M.A., and Kraker, G.P. 1981. Irradiation of samples for ^{40}Ar–^{39}Ar dating using the Geological Survey TRIGA reactor. US. Geological Survey, Professional Paper 1176, 55 p.

DePaolo, D.J. 1988. Neodymium Isotope Geochemistry, An Introduction, Mineral and Rocks. 187 pp., Springer Verlag, New York, N.Y.

Desmet, A. 1994. Ophiolites et séries basaltiques crétacées des régions caraïbes et norandines: bassins marginaux, dorsales ou plateaux océaniques ? Unpublished Doctorate thesis in science, Université de Nancy 1, France.

Dick, H.J.B., Meyer, P.S., Bloomer, S., Kirby, S., Stakes, D., and Mawer, C. 1991. Lithostratigraphic evolution of an in situ section of oceanic layer 3. *In* Proceedings of the Ocean Drilling Program, scientific results. *Edited by* R.P. Von Herzen, P.T. Robinson et al. 118, College Station, Texas, pp. 439–537.

Dunkley, P.N., and Gaibor, A. 1998. Mapa geológico de la Cordillera Occidental del Ecuador entre 2°–3° S., escala 1/200.000. CODIGEM – Ministerio de Energía y Minas – British Geological Survey publications, Quito, Ecuador and Nottingham, UK.

Echeverria, L.M. 1980. Tertiary or Mesozoic komatiites from Gorgona Island, Colombia; field relations and geochemistry. Contributions to Mineralogy and Petrology, **73**: 253–266.

Feeley, T.C., Cosca, M.A., and Lindsay, C.R. 2002. Petrogenesis and Implications of Calc-Alkaline Cryptic Hybrid Magmas from Washburn Volcano, Absaroka Volcanic Province, USA. Journal of Petrology, **43**: 663–703.

Francheteau, J., Armijo, R., Cheminee, J.L., Hekinian, R., Lonsdale, P.F., and Blum, N. 1990. 1 Ma East Pacific Rise oceanic crust and uppermost mantle exposed by rifting in Hess Deep (equatorial Pacific Ocean). Earth and Planetary Science Letters, **101**: 281–295.

Francheteau, J., Armijo, R., Cheminee, J.L., Hekinian, R., Lonsdale, P.F., and Blum, N. 1992. Dyke complex of the East Pacific Rise exposed in the walls of Hess Deep and the structure of the upper oceanic crust. Earth and Planetary Science Letters, **111**: 109–121.

Gillis, K.M. 1996. Rare earth element constraints on the origin of amphibole in gabbroic rocks from site 894, Hess Deep. Ocean Drilling Program, 147, pp. 59–75.

Giret, A., and Beaux, F. 1984. Le pluton du Val Gabbro (îles Kerguelen), un complexe tholéiitique, témoin de l'activité de la paléo-ride Est-Indienne. Compte Rendu de l'Académie des Sciences, 299, **14**: 965–970.

Goossens, P.J., and Rose, W.I. 1973. Chemical Composition and Age Determination of Tholeiitic Rocks in the Basic igneous Complex, Ecuador. Geological Society of America Bulletin, **84**: 1043–1051.

Grégoire, M., Cottin, J.-Y., Giret, A., Mattielli, N., and Weis, D. 1998. The meta-igneous rocks granulite xenoliths from Kerguelen Archipelago: evidence of a continent nucleation in an oceanic setting. Contributions to Mineralogy and Petrology, **133**: 259–283.

Hall, A. 1987. Igneous Petrology. Longman Scientific & Technical Publications, Harrow, England, 573 p.

Hart, S.R., and Dunn, T. 1993. Experimental cpx / melt partitioning of 24 trace elements. Contributions to Mineralogy and Petrology, **113**: 1–8.

Hart, S.R., Blusztajn, J., Dick, H.J., Meyer, P.S., and Muehlenbachs, K. 1999. The fingerprint of seawater circulation in a 500-meter section of ocean crust gabbros. Geochimica and Cosmochimica Acta, **63**: 4059–4080.

Hauff, F., Hoernle, K., Van den Bogaard, P., Alvarado, G., and Garbe-Schönberg, D. 2000*a*. Age and geochemistry of basaltic complexes in western Costa Rica: Contributions to the geotectonic evolution of Central America. Geochemistry, Geophysics, Geosystems, 1.

Hauff, F., Hoernle, G., Tilton, G., Graham, W., and Kerr, A.C. 2000*b*. Large volume recycling of oceanic lithosphere over short time scales: geological constraints from the Caribbean Large Igneous Province. Earth and Planetary Science Letters, **174**: 247–263.

Hofmann, A.W., Jochum, K.P., Seufert, M., and White, W.M. 1986. Nb and Pb in oceanic basalts: new constraints on mantle evolution. Earth and Planetary Science Letters, **79**: 33–45.

Hughes, R.A., and Pilatasig, L.F. 2002. Cretaceous and Tertiary terrane accretion in the Cordillera Occidental of the Andes of Ecuador. Tectonophysics, **345**: 29–48.

Hughes, R.A., Bermúdez, R., and Espinel, G. 1999. Mapa geológico de la Cordillera Occidental del Ecuador entre 0°–1° S, escala 1 : 200 000, CODIGEM – Ministerio de Energía y Minas – British Geological Survey publications, Quito, Ecuador and Nottingham, UK.

Humphris, S.E. 1984. The mobility of rare earth elements in the crust. *In* Rare earth element geochemistry. *Edited by* P. Henderson. Elsevier, Amsterdam, The Netherlands, pp. 317–342.

Jacobsen, S.B., and Wasserburg, G.J. 1980. Sm–Nd isotopic evolution of chondrites. Earth and Planetary Science Letters, **50**: 139–155.

Jaillard, E., Ordonez, M., Benitez, S., Berrones, G., Jimenez, N., Montenegro, G., and Zambrano, I. 1995. Basin development in an accretionary, oceanic-floored fore-arc setting; southern coastal Ecuador during Late Cretaceous – late Eocene time. AAPG Memoir, **62**: 615–631.

Jaillard, E., Benitez, S., and Mascle, G.H. 1997. Les déformations paléogènes de la zone d'avant-arc sud-équatorienne en relation avec l'évolution géodynamique. Bulletin de la Société géologique de France, **168**: 403–412.

Jenner, G.A., Dunning, H.J.B., Malpas, J., and Brace, T. 1991. Bay of I slands and Little Port complex revisited: age, geochemical and isotopic evidence suprasubduction origin. Canadian Journal of Earth Sciences, **28**: 1635–1652.

Juteau, T., and Maury, R.C. 1997. Géologie de la croûte océanique. Pétroplogie et dynamique endogènes. Editeurs Masson, Paris, France, 36 p.

Juteau, T., Mégard, F., Raharison, L., and Whitechurch, H. 1977. les assemblages ophiolitiques de l'occident équatorien: nature pétrographique et position structurale. Bulletin de la Société géologique de France, **5**: 1127–1132.

Juteau, T., Ernewein, M., Reuber, I., Whitechurch, H., and Dahl, R. 1988. Duality of magmatism in the plutonic sequence of Sumail nappe, Oman. Tectonophysics, **151**: 167–197.

Kausar, A.B. 1998. L'Arc Sud Kohistan: Evolution Pétrologique et Distribution des Eléments et Minéraux du Groupe du Platine. Unpublished Doctorate thesis in Earth Sciences, Université Joseph Fourier, France.

Kempton, P.D., and Hunter, A. 1997. A Sr-, Nd-, Pb-, O-isotope study of plutonic rocks from MARK, Leg 153: implications for mantle heterogeneity and magma chamber processes. *In* Proceedings of the Ocean Drilling Program, scientific results. *Edited by* J.A. Karson, M. Cannat, D.J. Miller et al. Ocean Drilling Program, Leg 153, pp. 305–320.

Kerr, A.C., Marriner, G.F., Arndt, N.T., Tarney, J., Nivia, A., Saunders, A.D., and Duncan, R.A. 1996*a*. The petrogenesis of Gorgona komatiites, picrites and basalts: new field, petrographic and geochemical constraints. Lithos, **37**: 245–260.

Kerr, A.C., Tarney, J., Marriner, G.F., Klaver, G.T., Saunders, A.D., and Thirlwall, M.F. 1996*b*. The geochemistry and petrogenesis of the late-Cretaceous picrites and basalts of Curaçao, Netherlands Antilles: A remnant of an oceanic plateau. Contributions to. Mineralogy and Petrology, **124**: 29–43.

Kerr, A.C., Marriner, G.F., Tarney, J., Nivia, A., Saunders, A.D., Thirlwall, M.F., and Sinton, C.W. 1997*a*. Cretaceous basaltic terranes in western Colombia; elemental, chronological and Sr–Nd isotopic constraints on petrogenesis. Journal of Petrology, **38**: 677–702.

Kerr, A.C., Tarney, J., Marriner, G.F., Nivia, A., and Saunders, A.D. 1997*b*. The Caribbean–Colombian Cretaceous igneous province; the internal anatomy of an oceanic plateau. Geophysical Monograph, **100**: 123–144.

Kerr, A.C., Tarney, J., Nivia, A., Marriner, G.F., and Saunders, A.D. 1998. The internal structure of oceanic plateaus; inferences from obducted Cretaceous terranes in western Colombia and the Caribbean. Tectonophysics, **292**: 173–188.

Kerr, A.C., White, R.V., and Saunders, A.D. 2000. LIP Reading: Recognising Oceanic Plateaux in the Geological Record. Journal of Petrology, **41**: 1041–1056.

Kerr, A.C., Aspden, J.A., Tarney, J., and Pilatasig, L.F. 2002*a*. The nature and provenance of accreted oceanic terranes in western Ecuador; geochemical and tectonic constraints. Journal of the Geological Society (of London), **159**: 577–594.

Kerr, A.C., Tarney, J., Kempton, P.D., Spadea, P., Nivia, A., Marriner, G.F., and Duncan, R. 2002*b*. Pervasive mantle plume head heterogeneity: Evidence from the Late Cretaceous Caribbean-Colombian oceanic plateau. Journal of Geophysical Research, **107**(7).

Khan, M.A., Jan, M.Q., Windley, B.F., Tarney, J., and Thirlwall, M.F. 1989. The Chilas mafic-ultramafic igneous complex; the root of the Kohistan island arc in the Himalaya of northern Pakistan. *In* Tectonics of the western Himalayas. *Edited by* L.L. Malinconico Jr. and R.J. Lillie. Geological Society of America, Boulder, Colo., Special Paper 75-94.

Khan, M.A., Jan, M.Q., and Weaver, B.L. 1993. Evolution of the lower arc crust in Kohistan, N. Pakistan; temporal arc magmatism through early, mature and intra-arc rift stages. *In* Himalayan tectonics. *Edited by* P.J. Treloar and M.P. Searle. Geological Society, London, Special Publication, pp. 123–138.

Lapierre, H., Dupuis, V., Mercier de Lepinay, B., Tardy, M., Ruiz, J., Maury, R.C., Hernandez, J., and Loubet, M. 1997. Is the lower Duarte igneous complex (Hispaniola) a remnant of the Caribbean plume-generated oceanic plateau?. Journal of Geology, **105**: 111–120.

Lapierre, H., Bosch, D., Dupuis, V., Polvé, M., Maury, R.C., Hernandez, J., Monié, P., Yeghicheyan, D., Jaillard, E., Tardy, M., Mercier de Lépinay, B., Mamberti, M., Desmet, A., Keller, F., and Sénebier, F. 2000. Multiple plume events in the genesis of the peri-Caribbean Cretaceous oceanic plateau province. Journal of Geophysical Research, **105**: 8403–8421.

Lavenu, A., Noblet, C., Bonhomme, M.G., Egueez, A., Dugas, F., and Vivier, G. 1992. New K–Ar age dates of Neogene and

Quaternary volcanic rocks from the Ecuadorian Andes; implications for the relationship between sedimentation, volcanism and tectonics. Journal of South America Earth Sciences, **5**: 309–320.

Leake, B.E., Wooley Alan, R., Arps, C.E.S., Birch, W.D., Gilbert, M.C., Grice, J.D., Hawthorne, F.C., Kato, A., Kisch, H.J., Krivovichec, V.G., Linthout, K., Laird, J., Mandarino, J., Maresch, W.V., Nickel, E.H., Rock, N.M., Schumacher, J.C., Smith, D.C., Stephenson, N.C.N., Ungaretti, L., Whittaker, E.J.W., and Youzhi, G. 1997. Nomenclature of amphiboles. Report of the Subcommittee on Amphiboles of the International Mineralogical Association Commission on New Minerals and Mineral Names. European Journal of Mineralogy, **9**: 623–651.

Lebrat, M., Megard, F., Dupuy, C., and Dostal, J. 1987. Geochemistry and tectonic setting of pre-collision Cretaceous and Paleogene volcanic rocks of Ecuador. Geological Society of America Bulletin, **99**: 569–578.

Litherland, M., Aspden, J.A., and Jemielita, R.A. 1994. The metamorphic belts of Ecuador. British Geological Survey, Overseas Memoir 11, 147 p.

Mamberti, M. 2001. Origin and evolution of two distinct Cretaceous oceanic plateau accreted in Western Ecuador (South America): Petrological, geochemical and isotopic evidence. Unpublished thesis, Universities Lausanne–Grenoble, 241 p.

Mamberti, M., Lapierre, H., Bosch, D., Jaillard, E., Ethien, R., Hernandez, J., and Polvé, M. 2003. Accreted fragments of the Late Cretaceous Caribbean–Colombian Plateau in Ecuador. Lithos, **66**: 173–199.

Mattielli, N. 1996. Magmatisme et métasomatisme associés au panache des Kerguelen: Contribution de la géochimie des enclaves basiques et ultrabasiques. Thèse d'Université Libre de Bruxelles, Belgiques, 232 p.

Mahoney, J.J., Storey, M., Duncan, R.A., Spencer, K.J., and Pringle, M. 1993. Geochemistry and age of the Ontong Java Plateau. Geophysical Monograph, **77**: 233–261.

Morimoto, M. 1988. Nomenclature of pyroxenes. Mineralogy Magazine, **52**: 535–550.

Miyashiro, A. 1973. The Troodos ophiolitic complex was probably formed in an island arc. Earth and Planetary Science Letters, **19**: 218–224.

Neal, C.R., Mahoney, J.J., Kroenke, L.W., Duncan, R.A., and Petterson, M.G. 1997. The Ontong Java Plateau: Geophysical Monograph, **100**: 183–216.

Nicolas, A., Reuber, I., and Benn, K. 1988. A new magma chamber model based on structural studies in the Oman ophiolite. Tectonophysic, **151**: 87–105.

Pallister, J.S. 1984. Parent magmas of the Semail ophiolite, Oman. *In* Ophiolites and oceanic lithosphere. *Edited by* I.G. Gass, S.J. Lippard, and A.W. Shelton. Geological Society, London, Special Publication 13, pp. 63–70.

Parkinson, I.J., Arculus, R.J., McPherson, E., and Duncan, R.A. 1996. Geochemistry, tectonics and the peridotites of the northeastern Solomon Islands. EOS, Transactions of the American Geophysical Union, Fall Meeting, Abstract, p. 642.

Pearce, J.A, Lippard, S.J., and Roberts, S. 1984. Characteristics and tectonic significance of supra-subduction zone ophiolites. *In* Marginal basin geology. *Edited by* B.P. Kokelaar and M.F. Howells. Geological Society, London, Special Publication, 16, pp. 74–94.

Pedersen, R.B., Malpas, J., and Fallon, T. 1996. Petrology and geochemistry of gabbroic and related rocks from site 894, Hess Deep. Ocean Drilling Program, Leg 147, pp. 3–19.

Révillon, S. 1999. Origine and composition du Plateau Océanique Caraïbe. Unpublished Doctorate thesis in Earth Sciences, Université de Rennes 1, France.

Révillon, S., Arndt, N.T., Hallot, E., Kerr, A.C., and Tarney, J. 1999. Petrogenesis of picrites from the Caribbean Plateau and the North Atlantic magmatic province. Lithos, **49**: 1–21.

Révillon, S., Arndt, N.T., Chauvel, C., and Hallot, E. 2000. Geochemical study of ultramafic volcanic and plutonic rocks from Gorgona island, Colombia: the Plumbing system of an oceanic plateau. Journal of Petrology, **41**: 1127–1153.

Reynaud, C., Jaillard, E., Lapierre, H., Mamberti, M., and Mascle, G.H. 1999. Oceanic plateau and island arcs of southwestern Ecuador; their place in the geodynamic evolution of northwestern South America. Tectonophysics, **307**: 235–254.

Roeder, P.L., and Emslie, R.F. 1970. Olivine-liquid equilibrium. Contributions to Mineralogy and Petrology, **29**: 275–289.

Saunders, A.D., Marsh, N.G., and Wood, D.A. 1980. Ophiolites as ocean crust or marginal basin crust. a geochemical approach. *In* Ophiolites Conference 193-204, Nicosia, Cyprus. *Edited by* A. Panayiotou.

Saunders, A.D., Tarney, J., Kerr, A.C., and Kent, R.W. 1996. The formation and fate of large oceanic igneous provinces. Lithos, **37**: 81–95.

Shervais, J.W. 2001. Birth, death, and resurrection: The life cycle of suprasubduction zone ophiolites. *In* Geochemistry, Geophysics, Geosystems, 2, paper number 2000GC0000080.

Sinton, C.W., and Duncan, R.A. 1997. Nicoya Peninsula, Costa Rica: A single suite of Caribbean oceanic plateau magmas. Journal of Geophysical Research, **102**: 15 507 – 15 520.

Sinton, C.W., Duncan, R.A., Storey, M., Lewis, J., and Estrada, J.J. 1998. An oceanic flood basalt province within the Caribbean plate. Earth and Planetary Science Letters, **155**: 221–235.

Spadea, P., Delaloye, M., Espinosa, A., Orrego, A., and Wagner, J.J. 1987. Ophiolite Complex from La Tetilla, southwestern Colombia, South America. Journal of Geology, **95**: 377–395.

Storey, M., Mahoney, J.J., Kroenke, L.W., and Saunders, A.D. 1991. Are oceanic plateaus sites of komatiite formation? Geology, **19**: 376–379.

Sun, S.S., and McDonough, W.F. 1989. Chemical and isotopic systematics of oceanic basalts. *In* Magmatism in the ocean basins: implications for mantle composition and processes. *Edited by* A.D. Saunders and M.J. Norry. Geological Society, London, Special Publication 42, pp. 313–345.

Todt, W., Cliff, R.A., Hanser, A., and Hofmann, A.W. 1996. Evaluation of a ^{202}Pb–^{205}Pb double spike for high-precision lead isotope analysis. *In* Earth processes. Reading the isotopic code. *Edited by* A. Basu and S. Hart. American Geophysical Union, Washington D. C., pp. 429–437.

Vance, D., Stone, J.O.H., and O'Nions, R.K. 1989. He, Sr and Nd isotopes in xenoliths from Hawaii and other oceanic islands. Earth and Planetary Science Letters, **96**: 147–160.

White, W.M., Hofmann, A.W., and Puchelt, H. 1987. Isotope geochemistry of Pacific mid-ocean ridge basalt. Journal of Geophysical Research, **92**: 4881–4893.

White, W.M, Albarède, F., and Telouk, P. 2000. High-precision analysis of Pb isotope ratios by multi-collector ICP–MS. Chemical Geology, **167**: 257–270.

Wilson, M. 1989. Igneous Petrogenesis. A global tectonic approach. Chapman & Hall editors, London, UK., 446 p.

Zindler, A., and Hart, S. 1986. Chemical geodynamics. Earth and Planetary Science Letters, Annual Revue, **14**: 493–571.

Appendix A

Appendix appears on the following page.

Appendix A. Calculation of the liquid in equibrium with the cumulate peridotite and olivine gabbro.

$Nd_{rock} = Nd_{ol} * \%$ olivine + $Nd_{cpx} * \%$ clinopyroxene + $Nd_{plag} * \%$ plagioclase + $Nd_{liqu} * \%$ liquid.

Nd_{rock}, Nd_{ol}, Nd_{cpx}, Nd_{plag}, and Nd_{liqu} are the Nd contents (ppm) in whole rock, olivine, clinopyroxene, plagioclase (refer to Tables 2 and 3) and liquid. This was estimated for the 97SJ10 wehrlite as follows:

$Nd_{rock} = 0.7 * Nd_{ol} + 0.2 * Nd_{cpx} + 0.05 * Nd_{plag} + x * Nd_{liqu}$(1)

$Nd_{ol} = 0$

$Nd_{plag} = 0$

$Nd_{rock} = 0.2 * Nd_{cpx} + x * Nd_{liqu}$

Assuming that the isotropic gabbro represents the liquid of the San Juan suite, the Nd abundance of the liquid is 4 ppm.

$X = (Nd_{rock} - 0.2 * Nd_{cpx})/Nd_{liqu}$

$X = (0.32 - 0.2 * 0.6)/4 = 0.05$